Host cell factors involved in the replication cycle of Bunyamwera virus

Kate Amy Loveday

Submitted in accordance with the requirements for the

degree of Master of Science by Research

The University of Leeds

School of Molecular and Cellular Biology

September 2018

The candidate confirms that the work submitted is her own and that appropriate credit has been given where reference has been made to the work of others.

This copy has been supplied on the understanding that it is copyright material and that no quotation from the thesis may be published without proper acknowledgement.

Acknowledgements

Thank you to John for this opportunity and the continued support and guidance, and in particular for keeping me positive after each pull down. A big thank you to 8.61, especially everyone from the Barr group, for their endless help throughout this year, thank you all for being welcoming enough that I decided to stay for another 4 years. Thank you to Joe, for making me feel a whole lot more organised over the last month. A special thank you to Greg, for being there for me on the good and the bad days, the last month would have been near impossible without you. Finally, a huge thank you to my parents, for not always understanding what I'm doing but supporting me (emotionally and financially) every step of the way.

I would like to thank Dr. Stuart Armstrong from the University of Liverpool for producing the mass spectrometry data set and the preliminary data analysis in section 3.3.1. Thank you to Rachel George from the University of Leeds mass spectrometry department for providing protein identifications in section 3.3.5.

Abstract

The *Bunyavirales* order is made up of nine families containing segmented negative sense ssRNA viruses that are mainly transmitted by arthropods. Members of the order are capable of causing acute and fatal disease in humans, mammals and plants. Due to their segmented genomic nature, reassortment between co-infecting viruses can readily occur, resulting in the emergence of a novel and potentially highly pathogenic virus, such as Schmallenberg virus. The emergence of novel bunyavirus coupled with the increased incidence or re-emergence of previously characterised bunyaviruses is a potential threat to public health and agriculture. There are currently no approved vaccines or therapeutics targeted against any bunyaviruses specifically, and it is therefore imperative that such disease prevention strategies are developed.

Bunyamwera virus (BUNV) is the prototype virus for the *Peribunyaviridae* family and is the virus used throughout the present study to investigate the interactions between cellular factors and the viral nucleocapsid (N). The N protein is the most abundant protein expressed by all bunyaviruses and it is critical for the encapsidation of all three RNA segments to form ribonucleoproteins. Mass spectrometry analysis was performed to create a data set of cellular proteins that are potential interaction partners of BUNV N. These interactions were validated using immunological methods in an attempt to provide further understanding of the virus/host interactions for this important group of viruses. It was shown that BUNV N does not interact with actin or ACTN4 throughout the virus life cycle.

Contents

List of Figures

List of Tables

Abbreviations

5-EU	5-Ethynyl uridine
ACTN4	α-actinin 4
APS	Ammonium persulphate
bp	Base pairs
BSA	Bovine serum albumin
BSL	Biosafety level
BUNV	Bunyamwera virus
CCHFV	Crimean-Congo haemorrhagic fever virus
CMC	Carboyl-methyl cellulose
DAPI	4'6-diamidino-2-pheylindole
DMEM	Dulbecco's modified eagle's media
FBS	Foetal bovine serum
GLB	Glasgow lysis buffer
HAZV	Hazara virus
hpi	Hours post infection
HSP70	Heat shock protein 70
HTNV	Hantaan virus
IAV	Influenza A virus
IF	Immunofluorescence
IFN	Interferon
IP	Immunoprecipitation
jpk	Jassplaskinolide
LACV	La Crosse virus
LDS	Lithium dodecyl sulphate
L segment	Large segment
MOI	Multiplicity of infection

mRNA	Messenger RNA
M segment	Medium segment
N	N protein
ORF	Open reading frame
PABP	Poly(A) binding protein
PBS	Phosphate buffered saline
PBS-T	PBS with Tween
PFA	Paraformaldehyde
pfu	Plaque forming units
PUUV	Puumala virus
PVDF	Polyvinylidene fluoride
RdRp	RNA dependent RNA polymerase
RER	Rough endoplasmic reticulum
RISC	RNA-induced silencing complex
RNA	Ribonucleic acid
RNAi	RNA interference
RNAPII	RNA polymerase II
RNP	Ribonucleoprotein complex
RT-PCR	Reverse transcription polymerase chain reaction
RVFV	Rift valley fever virus
SBV	Schmallenberg virus
SFM	Serum free media
SFTS	Severe fever with thrombocytopenia syndrome
SFTSV	SFTS virus
siRNA	Small interfering RNA
SNV	Sin Nombre virus
S segment	Small segment
ssRNA	Single stranded RNA
UTR	Untranslated region
vRNA	Viral RNA

Chapter 1

Introduction

1.1 Overview of the *Bunyavirales* Order

The *Bunyavirales* order (generic: bunyaviruses) comprises over 500 enveloped viruses that are categorised within Group V of the Baltimore classification system, as they have tripartite, negative sense single stranded RNA (ssRNA) genomes. In recent years the taxonomy of bunyaviruses has been revised and the old family, *Bunyaviri-dae*, has been reclassified as a new order, *Bunyavirales*, by the International Committee for Taxonomy of Viruses (ICTV)[54]. This taxonomic review has allowed for nine new families to be created, accommodating and separating the recently apparent diversity within the order (roughly 350 viruses that were previously unassigned to a genus)[49]. The families comprise: *Tospoviridae*, *Hantaviridae*, *Phasmaviridae*, *Phenuiviridae*, *Nairoviridae*, *Fimoviridae*, *Peribunyaviridae*, *Jonviridae* and *Feravir-dae*.

Viruses across the *Bunyavirales* order are known to infect a wide range of hosts, across animals, humans, insects and plants. The *Tospoviridae* family is the only family within the order to contain viruses that infect plants. The majority of bunyaviruses are arboviruses and are amplified in non-vertebrate vectors, such as ticks, thrips, mosquitos, sandflies and midges[83]. Members of the *Hantaviridae* family differ from the rest of the order because they are amplified and transmitted via rodents rather than arthropods, although there is some evidence to suggest hantaviruses may also be transmitted by non-rodent insectivores[27,73].
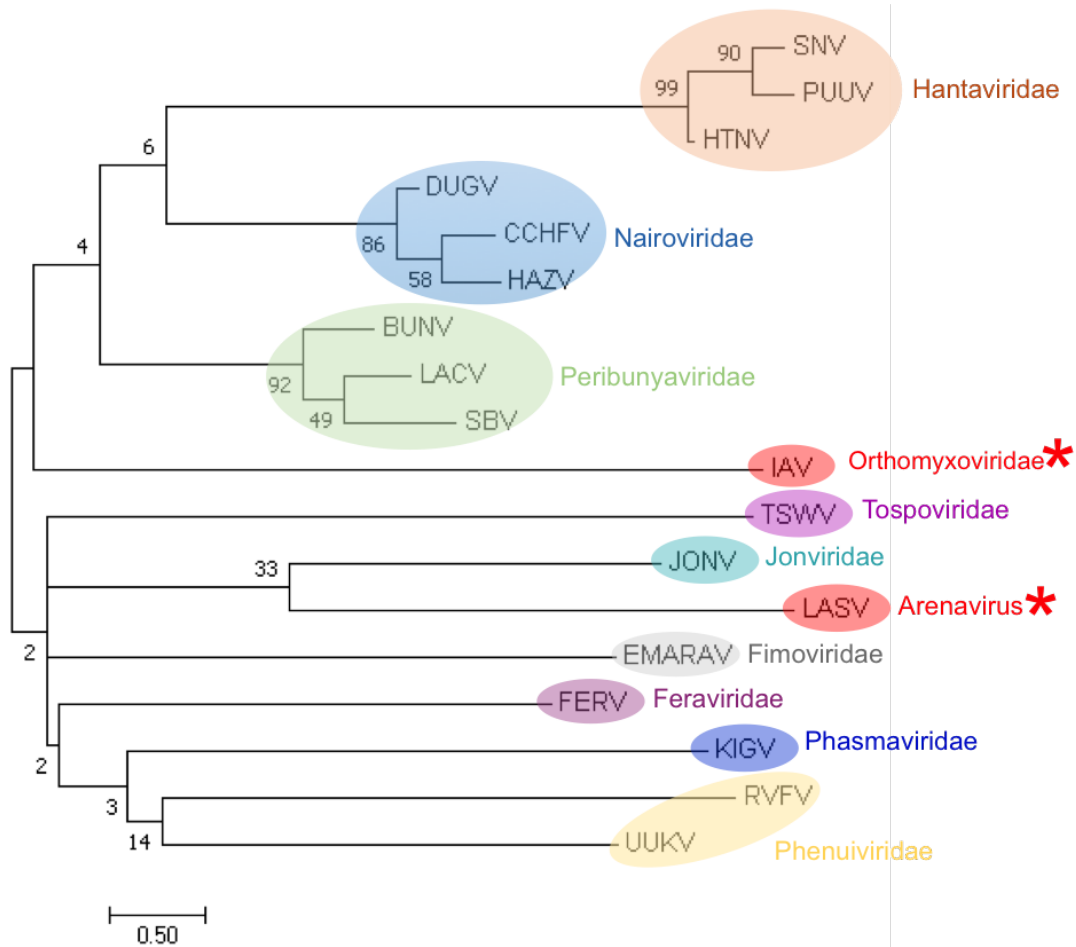
Figure 1.1: Molecular Phylogenetic analysis based on the N protein sequence of members from each *Bunyavirale* family.

The evolutionary history was inferred using the Maximum Likelihood method based on the JTT matrix-based model[39]. The tree with the highest log likelihood (-9258.47) is shown. The percentage of trees in which the associated taxa clustered together is shown next to the branches. Initial tree(s) for the heuristic search were obtained automatically by applying Neighbor-Join and BioNJ algorithms to a matrix of pairwise distances estimated using a JTT model, and then selecting the topology with superior log likelihood value. The tree is drawn to scale, with branch lengths measured in the number of substitutions per site. The analysis involved 18 amino acid sequences. All positions containing gaps and missing data were eliminated. There were a total of 211 positions in the final dataset. Evolutionary analyses were conducted in MEGA7[44].

Many bunyaviruses can be classified as emerging viruses due to their increased incidence and/or their emergence in a new geographical area. Emergence is often linked to new interactions between vector and host, and one driver of this is climate change. An increase in temperature can lead to the survival and reproduction of vec-

tors (thrips, ticks, mosquitos and mites) in areas where they previously would have been unable to live. It is inevitable that arthropod-borne diseases will eventually follow their vector into the new geographical area[88]. A new host population will be immunologically naïve to the emerging virus due to a lack of previous exposure, making individuals highly susceptible to the onset of disease.

The emergence of new viruses within a population can also be due to a significant change in virus genetics. Due to their tripartite genomic nature, bunyaviruses are susceptible to reassortment events, known as genetic shift. This can occur between both homotypic (same species) and heterotypic (same family) viruses, providing they are genetically compatible, share geographical distribution and/or a susceptible vector. Co-infection of a host with genetically related bunyaviruses can result in a mixing of segments and the emergence of a novel pathogen with the ability to cause severe disease in the host. During an outbreak of haemorrhagic fever in East Africa between 1997 and 1998 two isolates were discovered that were previously unidentified, named Garissa and Ngari virus. Sequence analysis determined that Ngari virus was a natural reassortment and that the small (S) and large (L) segments originated from Bunyamwera virus (BUNV)[14]. Interestingly, these two segments were nearly identical to those of Garissa virus, and it was determined that Garissa virus was not a novel bunyavirus but, in fact, an isolate of Ngari virus. The sequence of the medium (M) segment did not match any previously characterised members of the former *Orthobunyavirus* genus. In 2006, Briese *et al.* determined that Batai virus was the donor of the M segment[17].

More recently, a novel virus, named Schmallenberg virus (SBV), was first isolated in Germany in 2011 from cattle suffering with fever, decreased milk production and diarrhoea[35]. Metagenomic analysis confirmed that the same virus was later isolated from deformed newborn ruminants and determined as the causative agent for this disease. Sequence analysis revealed that the S and L segments from SBV originated from Shamonda virus, whereas the M segment matched more closely with Sathuperi virus, and confirmed that SBV was a natural reassortant[86]. Two years after the initial reports of SBV the majority of countries within Europe had known cases

of SBV, from Scotland to Eastern Europe (e.g. Slovenia)[28]. The origin of SBV is unclear and it is not fully understood how the virus spread into Europe, however, it is known that it is transmitted via biting midges (*Culicoides* spp)[78]. It is possible that SBV was carried into Europe by infected midges that were imported unknowingly with domesticated animals. Another theory suggests that the virus entered Europe within a reservoir and novel interactions with the vector and naïve hosts lead to the emergence of disease[78].

There are several viruses across the families that are responsible for severe disease in humans, and are most commonly associated with haemorraghic fevers. Crimean-Congo haemorrhagic fever virus (CCHFV) is a member of the *Nairoviridae* family that is transmitted by ticks and is responsible for haemorrhagic fever in infected humans, which has high fatality. CCHFV is the most geographically widespread tick-borne human viral disease, and is now characterised as an emerging virus due to the increase in countries becoming endemic and the increase in disease incidents in previously known endemic countries[68].

Rift Valley fever virus (RVFV) primarily affects animals but it is also able to infect and cause disease in humans through direct or indirect contact with blood or organs originating from infected animals. The majority of Rift Valley fever cases in humans are mild with symptoms passing within 7 days, however, 1 % of patients can develop haemorrhagic manifestations that can turn fatal in 50 % of cases[61]. Fatality rates tend to differ between different epidemics, however, they tend to be below 1 % of cases. Infection with RVFV in domesticated animals, such as sheep, goats, camels and cattle, is far more pathogenic than human infections, causing a severe economic loss to farmers. 90 % of lambs infected with RVFV die and there is a 100 % abortion rate in infected pregnant ewes [WHO].

Severe fever with thromboctyopenia syndrome (SFTS) is a newly emerging infectious disease, with incident rates increasing significantly across Eastern Asia over the past decade. This disease presents itself with symptoms including fever, thrombocytopenia (low platelet count) and leukocytopenia (low leukocyte count), with fatality rates ranging from 6-40 %[59,90,40]. The causative agent for this disease

was first identified as a novel bunyavirus in China in 2009, and named SFTS virus (SFTSV), since the discovery of the virus it has been detected across South Korea and Japan[77,40]. It is now understood that SFTSV is transmitted via ticks that are known to most commonly feed on domesticated animals (such as cattle, sheep, dogs and chickens) and that many patients suffering with SFTS are identified as farmers[90,51]. Importantly, studies have shown that SFTSV is able to infect domesticated animals without the development of visible symptoms[51].

The ability for SFTSV to be readily transmitted between a wide range of domesticated animals and humans through a tick vector makes this virus a potential threat to human health. In 2013 an elderly woman was hospitalised following various symptoms, including nausea and the loss of appetite. Laboratory tests revealed she was suffering with thrombocytopenia and leukocytopenia, however, she never developed a fever[87]. On the 7th day of infection serum sample was collected and through reverse transcription polymerase chain reaction (RT-PCR) it was confirmed that she was infected with SFTSV. This case is of particular interest because the patient had no history of tick bites or skin breaks. Investigation into her living conditions revealed that there were rats and wild cats surrounding her house and it was presumed that SFTSV was transmitted directly to humans from animals[87].

As previously mentioned, hantaviruses are most commonly found in rodents, however, they can be transmitted to humans via aerosolized virus particles from rodent excrement and saliva. Hantaviruses are asymptomatic in rodents and are able to maintain a persistent infection with no overt effects on the rodents life, however, disease onset in humans is radically different. The most common hantaviruses associated with human disease are Hantaan virus, Seoul virus, Puumala virus and Sin nombre virus. Infection with these viruses can result in one of two disease syndromes: haemorrhagic fever with renal syndrome or hantavirus cardiopulmonary syndrome, the latter having a mortality rate of 50 %[55,83].

Alongside bunyaviruses causing severe and economically devastating diseases in human and livestock, members of the *Tospoviridae* family are transmitted via thrips and cause infection within crops, threatening global food supplies. Tomato spotted

wilt virus causes significant loss in yield and quality of produce from vegetables, legume and ornamental crops in almost every continent[58].

The most pathogenic (and economically) devastating viruses within the *Bunyavirales* are commonly associated with high biosafety levels (BSL), for example CCHFV and RVFV are BSL 4. Viruses that can be handled in BSL 2 containment are used as models for studying these more pathogenic members as it is more cost and time efficient. BUNV has a relatively limited pathogenecity in humans compared to other members of the *Peribunyaviridae* family and is known to cause an acute febrile illness in individuals, with common symptoms such as headache, pains and rashes. Children are much more likely to develop symptoms and immunocompromised individuals have a greater risk of developing severe encephalitis[24]. BUNV is therefore the prototype virus for this family[82]. For this reason, BUNV was chosen to carry out the following study into the interactions between bunyaviruses and the host cell.

1.2 Bunyavirus Genomic Organisation

As previously mentioned members of the *Bunyavirales* order share a similar genomic organisation; a tripartite, negative sense ssRNA genome. The three segments differ in size and are named accordingly; small (S), medium (M) and large (L). All three segments share the same arrangement of an open reading frame (ORF) flanked by untranslated regions (UTR) at both the 3' and 5' end. There is a complementary sequence at the start of the 3' UTR and the end of the 5' UTR, allowing the segment to potentially form a panhandle (held by Watson and Crick interactions)[6]. As well as acting as the promoter sequence for both transcription and replication[7], the UTRs are known to be important in a variety of other roles within the virus life cycle across the different families of the *Bunyavirales*, including the encapsidation of viral RNA (vRNA) and the packaging of ribonucleoproteins complexes (RNP) into virus particles[27].

The S segment encodes the nucleocapsid (N) protein and the S segment of BUNV has an overlapping ORF which encodes NSs, a non-structural protein. The M seg-

ment encodes a single polyprotein that is co-translationally cleaved into both the glycoproteins (Gc and Gn) and a second non-structural protein, NSm. The L segment encodes the RNA dependent RNA polymerase (RdRp).
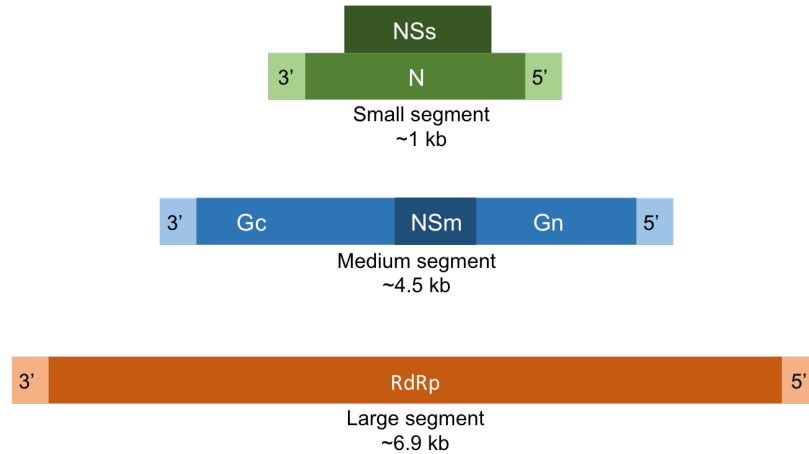
Figure 1.2: A schematic of BUNV genome segments.
The BUNV genome is comprised of three negative sense, ssRNA segments. Each segment has a 3' and 5' UTR at each end of the ORF. The small segment is 961 bp long and encodes the N protein, as well as NSs via a second initiation codon that results in an overlapping reading frame. The medium segment is 4458 bp and encodes Gc, NSm and Gn, these proteins are transcribed as a single polyprotein which is co-translationally cleaved by host proteases. The large segment is 6875 bp and encodes the RNA dependent RNA polymerase.

1.3 Bunyavirus Virion Structure

Bunyavirus particles have a relatively simple organisation and composition. There are only 4 structural proteins; the two surface glycoproteins (Gc and Gn), the N protein and the RdRp. The lipid envelope of the virus, derived from the host Golgi-apparatus, is coated in Gc-Gn heterodimers. The recent solution of high resolution structures of some of these glycoproteins suggest a greater diversity in virus structure amongst the order than first thought[27]. Members of the *Peribunyaviridae* family have glycoproteins that form a unique tripod arrangement of the virus surface. On the other hand, members of the *Hantaviridae* family have glycoproteins that form a distinctive tetrameric square-like lattice[10]. In contrast, the glycopro-

teins from members of the *Phenuiviridae* family form hexamers and pentamers, that together form an icosahedrally symmetrical virus particle. Within the virus particle, each ssRNA genomic segment is encapsidated by the N protein to form RNPs, which associate with the RdRp (shown schematically in figure 1.3). The internal endodomains of Gc/Gn glycoproteins are thought to interact with the RNP; this is thought to be a critical interaction required for virus assembly.
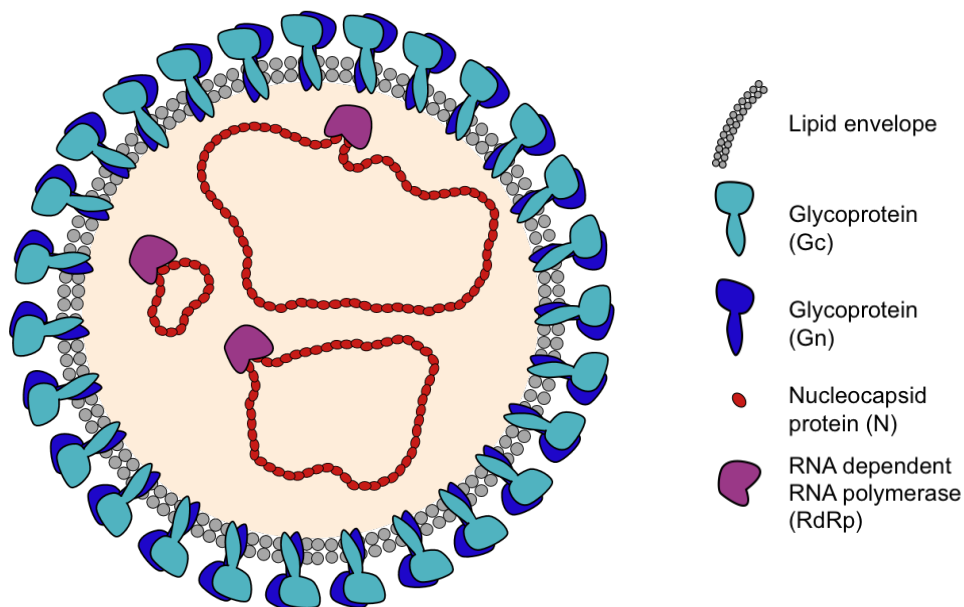
Figure 1.3: A schematic representation of a Peribunyaviridae virion.
The genome segments are encapsidated by the N protein to form RNPs. The RdRp associates with the viral RNP. The lipid envelope is derived from the host Golgi-apparatus and is coated in trimeric spikes of Gc-Gn heterodimers.

1.4 The Peribunyaviruses

Peribunyaviruses are one of the nine families belonging to the *Bunyaviridae* order. The family contains 200 viruses and consists of two genera; Orthobunyaviruses and Herbeviruses, which are further divided into 48 and 4 species (ICTV), respectively. Several viruses within this family are the causative agents of multiple diseases seen within humans, including acute febrile illness (Oropouche virus), haemorrhagic fever (Ngari virus) and encephalitis (La Crosse virus). Cache Valley virus, from the Or-

thobunyavirus serogroup, is known to cause abortions and abnormalities in offspring of ruminants[27]. BUNV is the prototype virus of the family, and its life cycle and molecular mechanisms are therefore well studied.
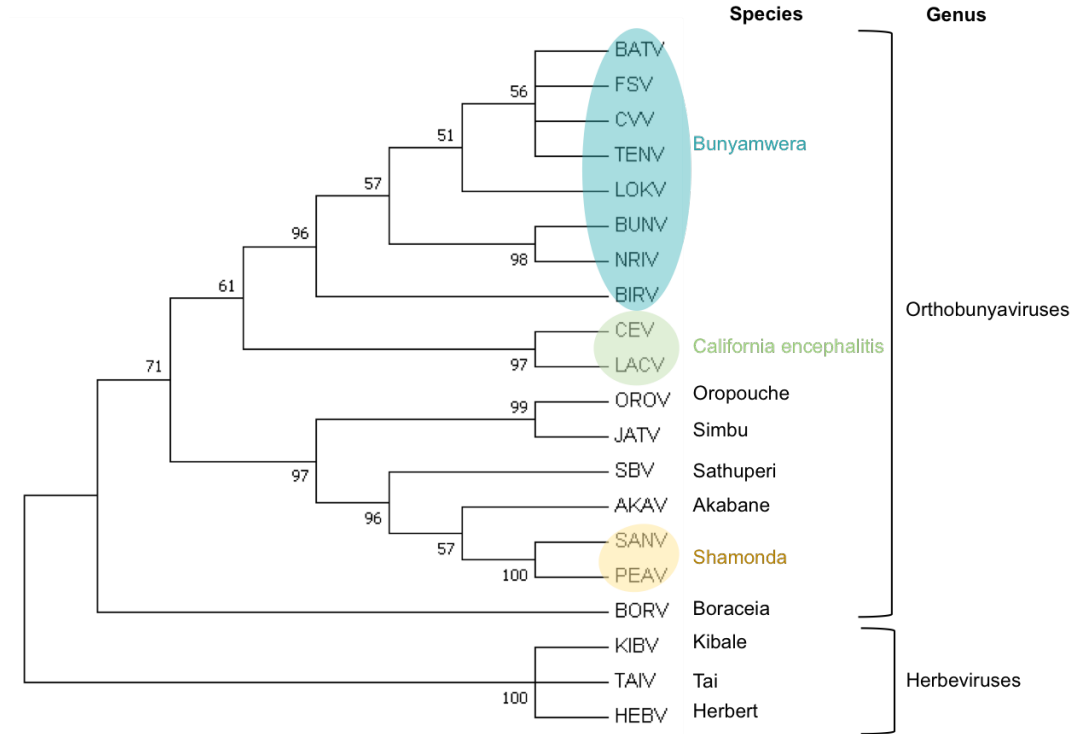
Figure 1.4: Molecular Phylogenetic analysis based on the N protein sequence from members of the *Peribunyaviruses*.
The evolutionary history was inferred by using the Maximum Likelihood method based on the Whelan And Goldman model[39]. The tree with the highest log likelihood (-4129.22) is shown. The percentage of trees in which the associated taxa clustered together is shown next to the branches. Initial tree(s) for the heuristic search were obtained automatically by applying Neighbor-Join and BioNJ algorithms to a matrix of pairwise distances estimated using a JTT model, and then selecting the topology with superior log likelihood value. A discrete Gamma distribution was used to model evolutionary rate differences among sites (5 categories (+G, parameter = 1.6480)). The analysis involved 20 amino acid sequences. All positions containing gaps and missing data were eliminated. There were a total of 218 positions in the final data set. Evolutionary analyses were conducted in MEGA7[44].

1.4.1 Nucleocapsid Protein

The nucleocapsid protein is the smallest structural protein expressed by BUNV, with its molecular weight being 26 kDa. The N protein associates with vRNA (genomes)

and cRNAs (antigenomes) along with the RdRp to form RNPs, with each N monomer binding 11 nucleotides (nt)[22]. The length of the BUNV genome comprises more than 13,000 nt, meaning that the N protein is highly abundant in the virus particle and within the infected cell. It is estimated that 1180 copies of N are needed to encapisdate all three segments, thus making the protein highly immunogenic[27]. In addition, N interacts with the glycoproteins during virus assembly in the Golgi (as shown in figure 1.6)[26].

The crystal structure for the N protein has been solved for several peribunyaviruses as a tetramer (including; BUNV, LACV, and SBV), and both bound and unbound to RNA[4,48,62]. The structure of peribunyaviral, hantaviral and nairoviral N proteins are all different, but all possess two major domains: the C-terminal domain and the N-terminal domain, which both have flexible arms. The centre of the tetramer is positively charged and binds to RNA. Each N monomer interacts with two neighbouring molecules, mediated by the N- and C- terminal arms to form a stable tetramer[47]. There is a continuous groove within the tetramer for RNA binding, ensuring that all the vRNA is fully encapsidated. The complete encapsidation of RNA by N prevents cellular RNase degrading the genome[56]. Rearrangement of the N protein must occur for the RdRp to transcribe vRNA.

1.4.2 Glycoproteins

The glycoproteins of BUNV are encoded as a single polyprotein (along with NSm) that is co-translationally transported into the endoplasmic reticulum, where it is cleaved into the 3 proteins by host proteases[83]. Gc is the largest glycoprotein, with a molecular weight of 110 kDa, whereas Gn is only 32 kDa in size. Both of the glycoproteins are type I integral membrane proteins that undergo N-linked glycosylation before forming a disulphide bond-linked heterodimers which are transported to the Golgi for virus assembly. The Gc/Gn dimer is also important in the maturation of viral particles and mediates the entry of viruses into host cells through receptor binding[83]. It has been shown that the transmembrane domain of Gn contains Golgi targeting and retention signals, and because of this the protein functions as a

chaperone of Gc[72]. Computational analysis of Gc suggests that it contains a class II fusion domain[31], also supported by mutational analysis of LACV and structural analysis of RVFV and Puumala virus (PUUV)[60,85,20]. The structure of class II fusion proteins shows that the protein is mostly comprised of β-sheets and contains a fusion loop of hydrophobic residues. Furthermore, it is believed that Gc is the primary glycoprotein involved in membrane fusion, as mutations surrounding the fusion loop in Gc led to a severe reduction in membrane fusion[69].

1.4.3   RNA dependent RNA polymerase

The RdRp is the largest protein of BUNV, with a molecular weight of ≈ 250 kDa. The primary role of the RdRp is to replicate the RNA segments and transcribe the S, M and L mRNAs required for subsequent protein translation[27]. There is an endonuclease domain within the N-terminus of the RdRp which is structurally related to that found in the polymerase of influenza A virus (IAV)[63]. This domain is responsible for the cleavage of 5' caps from host mRNAs, required for priming transcription. Whilst there is not a crystal structure for the RdRp of BUNV, the RdRp of LACV, a virus within the same genus as BUNV, has been solved, showing that it is similar in structure to that of IAV[32]. From this crystal structure it is understood that there are separate exit tunnels for the template and product, and moreover, the close proxomity of the entry and exit tunnel for the template allows for minimal disruption to the RNP during replication.

1.4.4   NSs

NSs is the smallest protein expressed by BUNV, with a molecular weight of 11 kDa, and is encoded by the S segment, it is translated from the same mRNA strand as N, but from a second initiation codon. This process is known as 'leaky' ribosome scanning, as the ribosome misses the first start codon and skips to the second[53]. It has been shown that the sequence surrounding the first start codon determines the levels of NSs, and that a suboptimal context of the first start codon results in

increased NSs expression. NSs is found to be localised in the cytoplasm and the nucleus[27]. NSs is non-essential to the BUNV life cycle, however, it plays a critical role in the pathogenesis of the virus[16,34].

The primary role of NSs in the BUNV life cycle is to aid in the evasion of the host antiviral immune response, through antagonising the Type I interferon (IFN) response[25]. It is understood that NSs of BUNV is able to block the phosphorylation of serine 2 in the C-terminal domain of cellular RNA polymerase II (RNAPII)[81], through interactions with Med8, a protein within the mediator complex[46]. This results in wide-spread shut off of host protein synthesis from RNAPII-dependent genes, including the gene encoding IFN-β, ultimately inhibiting the host antiviral response. Interesting, this characteristic of NSs is not seen within *Aedes Agypti* derived mosquito cells (C6/36) upon infection with BUNV[43], which may help the virus sustain a persistent infection in the arthropod vector.

Apoptosis is frequently induced by cells in order to prevent the spread of virus to naïve cells, so it is of no surprise that BUNV has evolved mechanisms to counteract this process. It has been shown that cells infected with BUNV not expressing NSs apoptose earlier than those infected with wildtype BUNV, but the exact mechanism that NSs uses to delay apoptosis remains unknown[34,41].

1.4.5   NSm

NSm is encoded by the M segment and its ORF is located in-between the two glycoproteins in the translated polyprotein. It is the second smallest protein encoded by BUNV, with a molecular weight of ≈ 18 kDa. NSm is predicted to have three hydrophobic and two non-hydrophobic domains, importantly two of these domains are non-essential, which has allowed for GFP be inserted at this site, creating a fluorescently labelled virus[70]. It is known that NSm has its own targeting signal in the N-terminus, and is localised to the virus factories within the Golgi complex[29,27]. This localisation suggests that NSm has functions in virus assembly and budding. Furthermore, it has been shown that NSm is a key factor, alongside actin, in viral tube assembly in the Golgi[29]. It is also suggested that NSm is a 'matrix' protein and

could be involved in the transport of RNPs to the cytosolic domains of glycoproteins accumulated in the Golgi (see figure 1.6). Deletion of NSm using reverse genetics has shown that NSm is not essential in the replication of infectious virions but the absence of NSm does result in a slower growth curve and reduced titres[70]. There are currently no characterised functions of NSm within arthropod cells[25].

1.5 Virus Life Cycle

BUNV is an arbovirus and is able to survive and replicate in both humans and mosquitoes, namely *Aedes aegypti*. Infection of BUNV in the human host results in a lytic infection and the onset of a mild febrile disease, known as Bunyamwera fever, whereas the virus is able to maintain a persistent[76], and systemic, infection within mosquitoes, with virus still being shed in the saliva months after the initially infection event[27]. Across other members of the *Bunyavirales*, it is believed that human infection is a dead-end event, with few cases of vertical transmission being confirmed[1], whereas it is known that vertical transmission occurs within mosquitoes[80,84].

BUNV is transmitted from an infected mosquito to a naïve human in the mosquito's saliva during a blood-meal, and vice versa from an infected human to a naïve mosquito in the human's blood. As mentioned above, BUNV is able to create a systemic infection within the vector; virions are first detected within the midgut of the mosquito, before the virus moves onto infect secondary organs. The saliva glands are the last organ to become infected by BUNV, and acts as the replication site, allowing BUNV to be transmitted to humans via the saliva during a blood-meal.

1.5.1 Virus Entry into Host Cells

Entry of BUNV into the host cell is controlled via interactions between the glycoproteins and host cell receptors, however the specific receptors have not yet been identified. The virus enters host cells via clathrin mediated endocytosis and is trafficked through the endosomal pathway where the changing biochemical environment

is critical in viral uncoating and RNP release into the host cell cytoplasm[36,65]. Once the RNP has been released into the cytoplasm, primary transcription occurs.

1.5.2 Replication, Transcription and Translation

Whilst the majority of research into the replication of BUNV has been carried out in mammalian cell lines, it is believed that the virus replicates in a similar manner in the mosquito vector as in the mammalian host. The RdRp is responsible for catalysing the transcription of negative sense RNA into positive sense mRNAs and genome replication. The transcription or replication of vRNA by the RdRp is determined by the presence of two distinct signalling sequences within the UTR, that are overlapping[6,7,8,9,42]. Both signals require terminal interaction; replication is not dependent on sequence specificity, however transcription is dependent on the presence of specific nucleotides at each terminal. There are common conserved nucleotides across all three segments of bunyaviruses as well as segment-specific sequences, both of these are important in determining the promoter strength for each segment[83].

Bunyaviral transcripts are primed using host-derived 5' caps, along with short oligoribonucleotide extensions that are derived from host cell mRNAs. This process is known as cap-snatching and as previously mentioned in section 1.4.3, it is mediated by an endonuclease domain within the N-terminal of the RdRp, which is structurally related to that found in the polymerase of IAV[63]. It is understood that these host cell mRNAs can have as little as 1 nt complimentary to that of the viral 3' template, and that a prime and align mechanism is used to select the host mRNAs and incorporate them into the template at the 3' end[30]. Each of the four structural and two non-structural proteins are translated from their respective mRNAs.
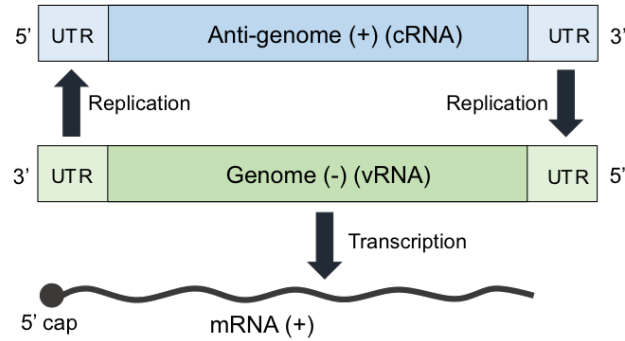
Figure 1.5: Schematic representation of BUNV negative sense gene expression
The negative sense genomic RNA is initially transcribed into mRNAs, which contain a host-derived 5' cap. The genomic RNA is replicated into a positive-sense anti-genomic intermediate that is transcriptionally silent. This intermediate is used as a template to generate nascent genomic RNA copies.

Once transcription has generated a pool of nascent mRNA transcripts, the viral RdRp switches its activity to that of a replicase. Whereas transcripts are naked and capped, the positive and negative sense replication products (vRNA and cRNA) are encapsidated by N, and are uncapped. It is not fully understood what causes the switch from viral transcription to replication, however, it is understood that the level of N protein is important, possibly to generate a sufficient amount of N protein available to encapsidate both the nascent anti-genomes and genomes throughout the replication process. It is notable that viral mRNAs lack the 3' poly(A) tails that are found on cellular mRNA. It is known that the BUNV S segment contains a sequence proximal to the 3' end that is important in translation enhancement[12]. Furthermore, there is a 3' stem loop present within the BUNV S segment that is similar in structure and sequence to stem loops found on cellular histone mRNAs, which are also known to lack a poly(A) tail. This suggests that BUNV is able to manipulate a cellular poly(A)-independent translation process to efficiently translate its own mRNAs. As mentioned in section 1.4.4 infection of BUNV results in host cell protein synthesis shut-off; the ability of BUNV to hijack an alternative translation mechanism would allow for the continual synthesis of viral proteins. Uniquely to bunyaviruses, transcription requires on-going translation, as the translation of nascent mRNAs prevents premature transcription termination[5].

1.5.3 Virus Replication Factory Formation

It is known that RNA viruses, as a whole, perform their biosynthetic events located on or within intracellular membranes. For this to be achieved, viruses are able to manipulate the cellular environment and organelle morphogenesis. It is understood that BUNV is able to form 'viral factories' around the Golgi of the host cell, providing the virus with a stable environment to evade the intracellular immune response. There are two main forms of viral factories during infection, factories formed during the early stages of infection ($\approx$ 5 hours post infection (hpi)) and those formed during the late stages of infection ($\approx$ 10 hpi). Within the early hours of infection, long tubular structures form within the Golgi, with a globular domain (Figure 1.6). These tubes are open to the cytoplasm to allow N to enter into the tubes, and the RdRp accumulates at the globular domain[29]. These early factories associate with the rough endoplasmic reticulum and mitochondria, the exact function of these interactions is unknown but it is believed that the cellular organelles provide factors required for viral replication[64,29]. Virus budding and assembly occurs in the factories seen during the late stages of infection, where no association with cellular organelles is seen. NSm and actin both function as scaffold proteins for the viral tubes. As previously mentioned, NSm contains a Golgi targeting signal, it is believed that NSm interacts with actin to help support the viral tubes[29].

1.5.4 Virus Assembly and Release

The co-translationally cleaved Gc and Gn proteins form a heterodimer within the endoplasmic reticulum before being transported to the Golgi complex. Here, they insert into the lipid membrane to create areas in the membrane that can support virus budding. The nascent RNPs are then translocated to the highly populated Gc-Gn regions of the Golgi membrane. It has been shown that direct interactions between the Gc-Gn tails and the RNPs are essential for effective budding into Golgi-derived vesicles[71]. This interaction between Gc-Gn and RNPs initiates changes in the Golgi morphogenesis, allowing the membrane to curve towards the lumen. Actin and NSm

help support this change in curvature and budding of newly assembled virus particles, and both proteins are present within these immature particles[29]. It has been shown that a functional trans-Golgi is imperative for virus maturation. transforming the annular immature particles into dense, compact structures[64]. It is also thought that NSm and actin are responsible for virus maturation, as both proteins are not present in the fully matured particles[29]. There are two main steps of maturation (type I and type II intracellular virions) before the final maturation into the virions that are released from the cell. The virus particles are trafficked through the exocytosis secretory pathway to the plasma membrane for release. It is currently unknown whether the virus undergoes the final step of maturation within the exocytic vesicle or during egress. This final maturation step causes the glycoprotein spikes to become more defined, ready for the virus to infect naïve cells[64,57].
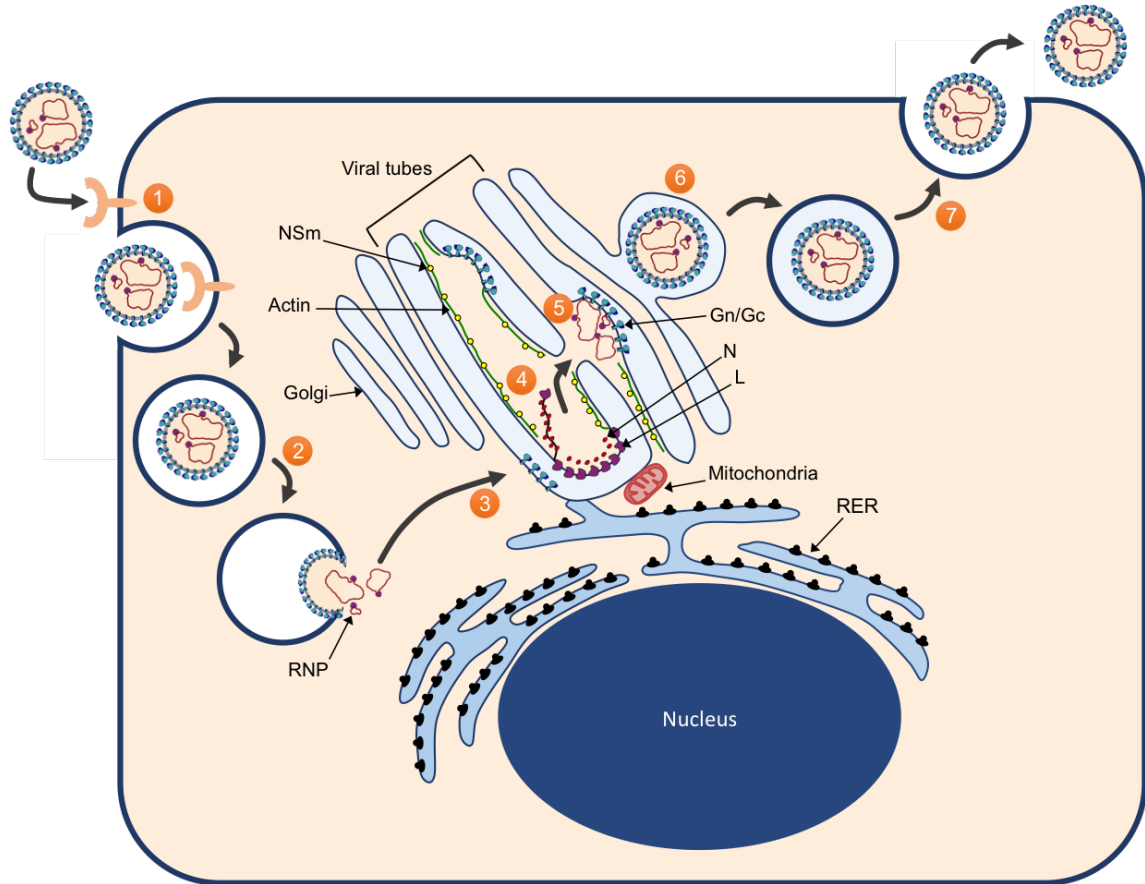
Figure 1.6: Schematic of the BUNV life cycle in mammalian cells.
1. BUNV binds to the host cell through unknown receptors and is endocytosed. **2.** The viral membrane fuses with the endosomal membrane and the RNPs are released into the cytoplasm.**3.** Viral factories are formed that are associated with the RER and mitochondira[29]. Actin and NSm act as a scaffold for the viral tubes. **4.** Transcription and replication of the viral genome occurs, with aid of host cell factors that are provided from the RER and mitochondria. Nascently replicated RNA is immediately encapsidated by N, forming RNPs. **5.** Actomyosin-based motors help transport these nascent RNPs through the cytoplasm, towards the cytoplasmic domains of the newly translated glycoproteins within the Golgi lumen. **6.** Immature virions are formed and undergo the first stages of maturation as they move through the trans-Golgi. **7.** Immature viruses go through the final maturation steps as they progress through the exocytosis secretory pathway. Mature virions are released.

1.5.5 BUNV in Arthropods

There has been limited research into the replication of BUNV within mosquito cells, but it is generally believed that replication occurs similarly to that of mammalian cells. In contrast to mammalian cells, BUNV is able to establish a persistent and

asymptomatic infection within mosquitoes, however, it is not fully understood how BUNV efficiently replicates for extended periods without causing adverse side effects. The RNAi response is the main anti-viral mechanism used by arthropods to inhibit viral replication[11]. Long double-stranded RNA is cleaved by a cellular riboendonuclease, Dicer-2, into double-stranded virus-derived small interfering RNAs (viRNAs) that are approximately 21 nt long. The RNA-induced silencing complex (RISC), in association with Argonaute-2, primes and activates the viRNAs so that one strand acts as a guide. This guide is able to bind to complementary ssRNA (such as mRNA), allowing RISC to cleave and degrade viral RNA, ultimately silencing viral protein synthesis[21]. It is no surprise that BUNV has evolved mechanisms to evade invertebrate anti-viral immune responses. It has been shown that NSs is essential for replication in cell lines that express an active Dicer-2 enzyme (U4.4 cell lines), but is not essential in cell lines that lack an RNAi response (C6/36 cell line). It is believed that an equilibrium between the RNAi response and virus replication is reached in order to allow for persistent infection, however further research is required to determine the role of NSs in this mechanism[27].

Likewise to BUNV replication in mammalian cells, BUNV is endocytosed into the cell, RNPs are released into the cytoplasm and viral replication factories form around the Golgi. In contrast to mammalian cells, these factories are smaller and less distinct[76]. During the early stages of infection with BUNV, mosquito cells form long projections that are believed to help try and 'seek' out neighbouring cells, however the true function of these projections remains unknown[52]. As mentioned above, viruses assemble and accumulate in the Golgi within mammalian cells, which causes disruptions to the Golgi[83]. Research has shown that BUNV does not cause disruptions to the Golgi during infection of moquito cells and the Golgi structure remains morphogenically similar to that of non-infected mosquito cells[52]. Instead, it is believed that the virus exits the cell immediately after it has assembled, rather than accumulating within the cell. Another difference between BUNV replication in mammalian cells and mosquito cells is the lack of host cell protein synthesis shut down within mosquitoes[16].

1.6   Host Cell Interactions with N

In addition to the ability of N to interact with the other viral components, there have been several studies carried out on members across the order showing that the N protein interacts with a variety of host cell proteins. Commonly, these interactions are essential for efficient virus replication and the production of nascent infectious particles. These multiple critical interactions make the N protein an attractive target for the development of therapeutics that would disrupt these interactions. Furthermore, targetting N would likely pose few off-target cytotoxic effects, as the hosts have no N protein homologs. Increased investigation into the interactions between N and host cell proteins throughout all aspects of the virus life cycle will aid in the development such of therapeutics as anti-virals.

Virus	Family	Host cell protein	Function	Source
CCHFV	*Nairoviridae*	HSP70	Protein folding	[75]
CCHFV	*Nairoviridae*	Actin	Cytoskeleton	[3]
CCHFV	*Nairoviridae*	eIF4G	Translation	[38]
CCHFV	*Nairoviridae*	MxA	Antiviral response	[2]
HAZV	*Nairoviridae*	HSP70	Protein folding	[75]
PUUV	*Hantaviridae*	Daxx	Apoptosis	[50]
HTNV	*Hantaviridae*	HSP70	Protein folding	[89]
HTNV	*Hantaviridae*	Importin α	Nuclear transport	[79]
SNV	*Hantaviridae*	S19	Ribosomal protein	[33]
BUNV	*Peribunyaviridae*	PABP	Translation	[12]

Table 1.1: Table of known interactions between bunyavirus nucleoproteins and host cell factors

1.6.1   HSP70

CCHFV is an emerging pathogen responsible for fatal haemorrhagic fever in infected humans, of which there is currently no known therapeutic. The relatively high mor-

tality rates and lack of preventive and therapeutic treatments means that CCHFV is classified as a hazard group 4 pathogen. CCHFV shares its serogroup with Hazara virus (HAZV), an apparently non-pathogenic virus to humans. The two viruses share similarities across their sequence, structure and replication cycle, enabling HAZV to be used effectively as a model to help study the biology of CCHFV in more depth. The crystal structure of both the HAZV and CCHFV N protein have previously been solved, revealing a close similarity between the two viral proteins[18,74]. This structural similarity further supports the use of HAZV as a model for CCHFV.

Surtees *et al.* have shown that the interactions between HAZV and CCHFV N protein and members of the HSP70 family are important in virus replication[75]. Initially, analysis of coprecipitating proteins was performed using mass spectrometry and the interacting proteins were further validated through immunological methods. This analysis discovered that cellular chaperones were interacting readily with the N protein, and in particular members of the HSP70 family. Using small inhibitory molecules against HSP70 activity, the group were able to show that these interactions were essential for efficient replication. The reduction in HSP70 activity resulted in a 1000-fold reduction in infectious HAZV particle production. Furthermore, it was shown that the HAZV-N interaction with HSP70 members occurred internally within the infected cells, as well as within released virus particles. Due to the similarity of the N protein structure between HAZV and CCHFV it is presumed that the same observations made during HAZV infection will also occur during CCHFV infection.

The interaction between N and HSP70 proteins has been reported for a broad range of negative stranded RNA viruses including rabies virus[45], measles virus[19] and Hantaan virus[89]. This is perhaps not surprising as members of the HSP70 family (when in association with another cellular cofactor, DnaJ) are important in assisting in correct folding and assembly of multicomponent complexes[67]. The RNPs of bunyaviruses, especially those from the *Nairoviridae* family[23], are large and therefore HSP70 may help in their folding.

1.6.2   PABP

Bunyaviral mRNAs lack the poly(A) tails that would usually be found at the 3' end of host cell mRNAs, important in the nuclear export, translation and stabilisation of mRNA. The poly(A) tail acts as a binding site for poly(A) binding protein (PABP), a protein that promotes export from the nucleus and prevents mRNA degredation. Efficient translation requires the recruitment of various transcription factors and related scaffolding proteins. Blakqori et al. used model mRNAs that mimic the organisation of BUNV S-segment mRNAs to investigate the effect of the UTRs on efficient translation, and if these regions were functionally similar to the canonical 3' poly(A) tail[12]. The study provided evidence that suggests the BUNV S mRNA 3' UTR is able to enhance mRNA translation in much the same way as a poly(A) tail, although the mechanism by which this occurs is unknown. Furthermore, the study showed that BUNV N is able to inhibit the translation of host polyadenylated mRNA by interacting with PABP. PABP was redistributed and retained in the nucleus following infection of cells with BUNV.

Previous studies have shown that the peribunyavirus non-structural protein, NSs, is responsible for host protein synthesis shut down[13,16] and redistribution of PABP to the nucleus, which occurred faster in cells expressing-NSs. However, viruses that did not express NSs were still able to cause a redistribution of PABP to the nucleus, suggesting other proteins are involved. BUNV N protein was found to bind and co-localise with PABP in the cytoplasm shortly after infection, followed by nuclear retention of PABP. This allows for the efficient translation of viral mRNA and the inhibition of host mRNA translation[12].

1.6.3   Actin

Through peptide mass finger printing it has been shown previously that actin is a key factor in the structure of viral tubes where viral replication factories are found[29]. After treatment of infected cells with jasplaskinolide (Jpk), a drug that stabilises filamentous actin, there were no intact viral tubes visualised in infected cells. The site

of viral assembly was displaced from perinuclear to the plasma membrane. Furthermore, treatment with Jpk lead to a 60-70% reduction in the production of infectious virus particles.

The mass spectrometry results produced by Surtees *et al.* showed that many interacting partners of CCHFV N were components of the cytoskeleton, including actin, tubulin and vimentin. This correlated with evidence from previous studies in which the importance of actin filaments in CCHFV assembly was first established[3]. In these experiments, CCHFV N was also shown to interact with actin through immunoprecipitation assay and Western blot analysis. The importance of actin filaments in the process of virus assembly was demonstrated by disrupting the actin filaments with Cytochalasin D, which resulted in a decrease of assembled virus.

1.7 Project Aims

Previous studies have shown that the nucleocapsid proteins of bunyaviruses interact with a variety of host cell proteins, and that disrupting these interactions can have a negative effect on viral replication or infectivity. This project aims to determine novel interactions between BUNV N and host cell proteins by developing a mass spectrometry data set and confirming the interactions through co-immunoprecipitation assays. The location of these interactions will also be determined using confocal microscopy. Understanding the interactions between N and host cell proteins throughout the virus life cycle will help to develop new therapeutics targeted against N.

Chapter 2

Materials & Methods

2.1   Materials

2.1.1   Continuous Human Cell Lines

SW13 cells are a human adrenal cortex carcinoma cell line, originally derived from a small cell carcinoma tissue biopsy. A549 cells are a human alveolar basal epithelial adenocarcinomal cell line. BHK-21 cells are derived from baby hamster kidney fibroblasts (American Type Cell Culture, ATCC).

2.1.2   Virus Strains

HAZV strain JC280 was kindly provided by Dr Stuart Dowall and Dr Roger Hewson (Public Health England, UK) as an infectious cell culture supernatant from SW13 cells. Wild type BUNV stocks were kindly provided by Samantha Hover (Leeds, UK), as an infectious cell culture supernatant from BHK-21 cells.

2.2   Methods

2.2.1   Cell Culture Methods

2.2.1.1   Continuous cell culture

All cell lines were maintained at 37 $^{\text{o}}$C with 5 % CO_2 in humidified incubators. All cell lines were grown in Dulbecco's Modified Eagle's Media (DMEM; Sigma) supplemented with 10 % foetal bovine serum (FBS; Invitrogen) and 100 IU penicillin/mL,

and 100 µG streptomycin/mL, this is referred to as complete media. Cell lines were passaged using trypsin (Sigma) as the cells were reaching 100 % confluency.

2.2.1.2   Freezing and Thawing Cells

Cell lines were frozen in liquid nitrogen for long term storage. Cells were trypsinised and resuspended in complete media before being washed three times in PBS, with centrifugation at 1000 xg at 4 $^{\circ}$C for 5 minutes after each wash. Cells were re-suspended in 10 % dimethyl sulphoxide, 40 % FBS and 50 % DMEM. 1 mL cell suspension was aliquoted into cryovials which were cooled to -80 $^{\circ}$C before being placed in liquid nitrogen. Cells were thawed rapidly at 37 $^{\circ}$C and transferred to a T25 cm^2 flask and supplemented with complete media. Cells were expanded once they had reached 80 % confluency and passaged at least twice more before being seeded for experiments.

2.2.2   Virological Techniques

2.2.2.1   Virus infection

Once cells had reached 70-80 % confluency complete media was replaced with serum free media (SFM) and infected with either BUNV/HAZV at multiplicity of infection (MOI) = 0.1 unless stated otherwise. Cells were incubated for 1 hour with rocking, cells were then washed twice with PBS and 2 % FBS DMEM was added. Infected cells were incubated at 37 $^{\circ}$C for the desired length of time.

2.2.2.2   BUNV Propagation

A549 cells were seeded into 2x T175 cm^2 flasks and incubated at 37 $^{\circ}$C until they were 80-90 % confluent. Complete media was removed off of the cells and replaced with 3 mL SFM and infected at MOI = 0.01. Cells were incubated for 3 hours at 37 $^{\circ}$C on a rocker. After 3 hours 9 mL of SFM was added and cells were incubated for 4 days at 37 $^{\circ}$C, the flasks were rocked by hand twice a day. At 96 hpi (hours post infection) the supernatant was collected and clarified by centrifuging at 375 x g

for 10 mins. Supernatant was aliquoted out and stored at -80 $^\text{o}$C. Virus titre was determined by plaque assay (see below).

2.2.2.3   BUNV Titre Determination by Plaque Assay

SW13 cells were seeded into a 6 well plate and incubated at 37 $^\text{o}$C until they were 90-95 % confluent. A serial dilution of BUNV was made, from 10^{-1} to 10^{-6} in SFM. Complete media was removed from cells and they were washed with PBS. Virus dilutions were added carefully to the cells and incubated at 37 $^\text{o}$C for 1 hour on a rocker. Complete media was diluted 1:1 with 1.6 % (w/v) high viscosity carboxyl-methyl cellulose (CMC, sigma). CMC prevents virus migrating through the media, ensuring that the secreted infectious virion from an infected cell could only infect immediately neighbouring cells. Plaques were formed due to BUNV infection resulting in cell lysis in very defined regions. Virus was removed from the cells, and complete media:CMC was added to the cells as an overlay. The cells were incubated at 37 $^\text{o}$C for 7 days. Cells were fixed and stained simultaneously by adding fix/stain solution (12.5 % formaldehyde, 20 % ethanol and 0.1 % (w/v) crystal violet solution), directly into media/CMC. The chromophore containing component of crystal violet binds to the negatively charged cell membranes (it is positively charged at pH 7). Healthy cells appears purple in the plaque assay, and areas where the virus has caused lysis appear transparent as they are not stained. Cells were incubated for 30 mins - 1 hour, the fix/stain was removed and cells were washed thoroughly with dH$_2$O, and allowed to dry. The following equation was used to determine virus titre:

$$\textbf{Virus titre (PFU/mL)} = \frac{\textbf{Number of plaques}}{\textbf{dilution factor x volume (mL)}}$$

2.2.3 Analysis of Protein Expression

2.2.3.1 Preparation of Whole Cell Lysate

Cells were harvested by scraping whilst in media. The suspended cells were centrifuged at 4 $^{\circ}$C at 2000 x g for 5 minutes. Cells were washed twice in PBS, with the same centrifugation step inbetween each wash. The cell pellet was finally resuspended in lysis buffer (10 mM Tris-HCl pH 7.5, 150 mM NaCl, 0.5 mM EDTA, 0.5 % NP40, 1 x EDTA-free complete protease inhibitor) for immunoprecipitation and Glasgow lysis buffer (GLB) (20 mM PIPES, 240 mM KCl, 60 mM NaCl, 10 mM MgCl$_2$, 2 % Triton x-100, 20 % glycerol, 1 x EDTA-free complete protease inhibitor) for the 72 hour time courses. Cells were incubated in lysis buffer on ice for 30 minutes. Cell lysates were clarified by centrifugation at 13,000 x g at 4 $^{\circ}$C for 10 minutes. The pellet was discarded and the supernatant containing total protein was either used immediately or stored at -80 $^{\circ}$C for future use.

2.2.3.2 SDS Polyacrylamide Gel Electrophoresis (SDS PAGE)

SDS PAGE gels were made with a 12 % resolving gel (4 mL 30 % bis-acrylamide, 2.5 mL 1.5 M Tris-HCl pH 8.8, 3.3 mL ddH$_2$O, 100 µL 10 % SDS, 100 µL 10 % ammonium persulphate (APS), 10 µL TEMED) and 5 % stacking gel (0.83 mL 30 % bis-acrylamide, 0.63 mL 1 M Tris-HCl pH 6.8, 3.4 mL ddH$_2$O, 50 µL 10 % SDS, 50 µL 10 % APS, 5 µL TEMED). Protein samples were mixed 4 x LDS (lithium dodecyl sulphate) sample buffer (1 x LDS; 106 mM Tris HCl, 141 mM Tris Base, 2 % LDS, 10 % glycerol, 0.51 mM EDTA, 0.22 mM G250 Coomassie Blue, 0.157 mM phenol red; pH 8.5), supplemented with 50 mM DTT reducing agent. Samples were heated at 95 $^{\circ}$C for 5 minutes to denature the proteins and allowed to cool before loading onto the gel. Samples were loaded alongside color prestained, protein standard, broad range ladder (New England Biolabs). Electrophoresis was performed in SDS running buffer (25 mM Tris, 192 mM glycine, 0.1 % (w/v) SDS) at 180 V for 50-80 minutes (until the dye front had run off the gel).

2.2.3.3 Western Blot Analysis

Proteins were transferred from the SDS PAGE gels to a fluorescence compatible polyvinylidene fluoride (PVDF) membranes (Immobolin-FL transfer membrane; Millipore) using a Trans-Blot semi-dry cell (Bio-rad) in Towbin buffer (25 mM Tris, 192 mM glycine, 20 % methanol) for 1 hour at 15 V. The membranes were blocked for 1 hour at room temperature in 50 % Odyssey blocking buffer (LiCor) in PBS. The membranes were then incubated with primary antibody diluted to the appropriate concentration in 50 % Odyssey blocking buffer in PBS, for either 1 hour at room temperature or overnight at 4 $^{\circ}$C. The membranes were washed 3 x in PBS before incubating with the appropriate fluorescent secondary antibody diluted in 50 % Odyssey blocking buffer in PBS, for 1 hour at room temperature. The membranes were washed 3 x in PBS and allowed to dry before using a LiCor Odyssey Sa Infrared imaging system (LiCor) to directly visualise the membranes.

2.2.3.4 Protein Visualisation by Coomassie, InstantBlue and Silver Stain

Proteins that had been resolved by SDS PAGE were visualised by incubating gels in Coomassie stain (0.25 % (w/v) Coomassie R-250, 50 % (v/v) methanol, 10 % (v/v) glacial acetic acid) at room temperature for 1 hour. The gels were destained for 1 hour at room temperature using destain solution (40 % (v/v) methanol, 10 % (v/v) glacial acetic acid) and rehydrated in ddH$_2$O prior to imaging. For protein identification (section 3.3.5) proteins were visualised using InstantBlue (Expedon). Gels were incubated with InstantBlue for 15 minutes whilst rocking and then moved into water once stained. InstantBlue requires no fixing, washing or destaining steps. Gels were silver stained using a SilverQuest staining kit (Invitrogen) according to the manufacturer's instructions.

2.2.3.5 Immunofluorescence (IF)

In order to visualise the subcellular localisation of host and viral proteins, IF experiments were performed. Cells were grown on 19mm glass coverslips housed in 12 well

plates prior to infection and later fixation. Media was removed from the cells and they were washed twice in PBS. Cells were fixed to the glass coverslips by adding 4 % (w/v) paraformaldehyde (PFA) for 20 minutes at room temperature. After PFA was removed from the cells, they were washed 3 times with PBS and stored in PBS at 4 °C until future use, or permeabilised in 0.5 % (v/v) Triton-X 100 in PBS for 10 minutes at room temperature. After permeabilisation, cells were washed 3 times and blocked in 1 % (w/v) bovine serum albumin (BSA) in PBS for 15 minutes at room temperature. The cells were incubated with primary antibodies at the appropriate dilution in 1 % (w/v) BSA in PBS overnight at 4 °C. The cells were washed 3 times in PBS, prior to the addition of the fluorescent secondary antibody (made up to the appropriate dilution in 1 % BSA in PBS), the cells were incubated for 1 hour at room temperature blocked from the light. Cells were washed 3 times in PBS, and then incubated with DAPI (4'6-diamidino-2-pheylindole) (Invitrogen) diluted 1:10,000 in dH_2O, for 3 minutes to allow for cell nuclei visualisation. Cells were washed 5 times in PBS before mounting onto coverslips with VectaSheild mounting medium (Vector Laboratories). Mounted coverslips were stored at 4 °C for long term storage. Confocal images were captured using an Zeiss LSM700 Inverted with Airyscan microscope.

2.2.4 Immunoprecipitations

2.2.4.1 Dynabead IPs

Dynabeads coupled to recombinant Protein G were used to IP the appropriate protein of interest from cell lysates, using an antibody specific for the protein of interest. Dynabeads are uniform, 2.8 µm superparamagnetic beads with recombinant Protein G covalently conjugated to their surface. Protein G is a bacterial protein which binds to the Fc region of most mammalian antibodies. 50 µL Dynabeads were transferred to a 1.5 mL microfuge tubes and placed on a magnetic rack, the beads migrated to the side of the tube facing the magnet and the supernatant was removed and replaced with the appropriate antibody diluted 1:100 in 200 µL of Ab Binding and

washing buffer (Life Technologies). The beads and antibody mix were incubated with rotation for half an hour at room temperature to allow the antibody to bind to Protein G. Tubes were placed on a magnetic rack and the supernatant containing unbound antibodies was removed. The Ab bound beads were washed twice in Ab binding and washing buffer. Cell lysates were prepared as described in section 2.2.3.1 and incubated with the Ab bound Dynabeads overnight at 4 ^{o}C with rotation. Tubes were placed on a magnetic rack and the supernatant containing the unbound proteins from the cell lysate was saved for later analysis via Western blot.

Dynabeads with antibody-antigen complexes were washed 3 times in filtered PBS with Tween (PBS-T, 0.1 % Tween-20) during the fourth wash with PBS-T the Dynabeads were moved into a clean microfuge tube to eliminate the elution of proteins that may be bound to the side of the tube. At each wash stage the supernatant was removed and saved for later analysis. The Dynabeads with antibody-antigen complexes were incubated for 5 minutes in 20 μL Elution buffer (Life Technologies) at room temperature to elute the antibody-antibody complexes from Protein G coupled Dynabeads. Tubes were placed on a magnetic rack and the supernatant containing the eluted proteins was removed and saved for analysis via Western blot as described in 2.2.3.3.

2.2.5 Mass Spectrometry

2.2.5.1 SDS-PAGE

Eluted proteins were separated on a NuPAGE®(Life Technologies) precast 4-12 % gel Tris-Bis gradient gel and the proteins were stained with colloidal Coomassie Blue G-250 (Simply Blue^{TM}, Life Technologies) according to the manufacturer's instructions.

2.2.5.2 Tryptic digestion

The entire gel lane (avoiding antibody chain bands) was excised and cut into smaller pieces ($\approx$ 1mm^3). Gel pieces were destained in 50 % acetonitrile/50 mM ammonium

bicarbonate (pH $\approx$ 8), reduced for 30 minutes at 37$^\text{o}$C with 10 mM dithiothreitol (Sigma) in 50 mM ammonium bicarbonate and alkylated with 55 mM iodoacetamide (Sigma) in 50 mM ammonium bicarbonate for 30 minutes in the dark at room temperature. Gel pieces were washed for 15 minutes in 50 mM ammonium bicarbonate and dehydrated with 100 % acetonitrile. Acetonitrile was removed and the gel plugs rehydrated with 0.01 μg/μL proteomic grade trypsin (Sigma) in 50 mM ammonium bicarbonate. Digestion was performed overnight at 37 $^\text{o}$C. Peptides were extracted from the gel plugs using successive 15 minute incubations of 50 % (v/v) acetonitrile 0.1 % (v/v) TFA. Peptide extracts were pooled and reduced to dryness using a centrifugal evaporator (Eppendorf concentrator plus) and re-suspended in 3 % (v/v) acetonitrile, 0.1 % (v/v) TFA for analysis by mass spectrometry.

2.2.5.3 NanoLC MS ESI MS/MS analysis

Peptides were analysed by on-line nanoflow LC using the Ultimate 3000 nano system (Dionex/Thermo Fisher Scientific) essentially as described by Bricio-Moreno et al (2018)[15]. Samples were loaded onto a trap column (ThermoScientific, PepMap100, C18, 300 μm x 5 mm) then resolved on an analytical column (Easy-Spray PepMap® RSLC 50 cm x 75 μm inner diameter, C18, 2 μm, 100 Å) fused to a silica nano-electrospray emitter (Dionex). The column was operated at a constant temperature of 30$^\text{o}$C and the LC system coupled to a Q-Exactive HF mass spectrometer (Thermo Fisher Scientific). Chromatography was performed with a buffer system consisting of 0.1 % formic acid (buffer A) and 80 % acetonitrile in 0.1 % formic acid (buffer B). The peptides were separated by a linear gradient of 3.8 – 50 % buffer B over 30 minutes at a flow rate of 300 nl/min. The Q-Exactive HF was operated in data-dependent mode with survey scans acquired at a resolution of 60,000 and scan range 350-2000 m/z. Up to 10 of the most abundant isotope patterns with charge states +2 to +5 from the survey scan were selected with an isolation window of 2.0 Th and fragmented by higher energy collisional dissociation with normalized collision energies of 30. The maximum ion injection times for the survey scan and the MS/MS scans were 100 and 45 ms respectively, and the ion target value was set to 3E6 for survey scans and

1E5 for the MS/MS scans. MS/MS events were acquired at a resolution of 30,000. Repetitive sequencing of peptides was minimized through dynamic exclusion of the sequenced peptides for 20 s.

2.2.5.4 Bioinformatic analysis

Spectral data were analysed using the PEAKS studio 8.5 software (Bioinformatics Solutions Inc., Waterloo, ON, Canada). Tandem MS data were searched against the predicted protein sets of BUNV (Uniprot, Aug 2018) and Human (Uniprot, Aug 2018, 3AUP000005640) (73186 sequences combined). Search parameters were as follows; precursor mass tolerance set to 10 ppm and fragment mass tolerance set to 0.01 Da. Two missed tryptic cleavages were permitted. Carbamidomethylation (cysteine) was set as a fixed modification and oxidation (methionine) was set as a variable modification. The false discovery rate was set at 1 %.

2.2.6 List of Antibodies

Target	Supplier	Catalogue number	WB dilution	IF dilution
BUNV N	In house	N/A	1:10,000	1:1,000
HAZV N	In house	N/A	1:10,000	N/A
GAPDH	Abcam	ab8245	1:10,000	N/A
HSP70	Abcam	ab6535	1:1,000	N/A
Actin	Sigma Aldrich	A3853	1:10,000	N/A
ACTN4	Abcam	ab108198	1:1,000	1:100
PABP	Abcam	ab12060	1:1,000	N/A

Table 2.1: Table of primary antibodies used in Western blot analysis and IF staining

Primary antibody species	Conjugation	Supplier	Catalogue number	WB dilution	IF dilution
Mouse	IRDye 680CW	LiCor	925-68072	1:20,000	N/A
Rabbit	IRDye 800CW	LiCor	25-32213	1:20,000	N/A
Sheep	IRDye 800CW	LiCor	925-32214	1:20,000	N/A
Rabbit	Alexa Fluor 488	Invitrogen	A-21441	N/A	1:500
Sheep	Alexa Fluor 633	Invitrogen	A-21082	N/A	1:500

Table 2.2: Table of secondary antibodies used in Western blot analysis and IF staining

Chapter 3

Results

3.1   BUNV Propagation

In order to propagate BUNV and generate a stock of known titre for all future experiments, A549 cells were infected at an moi of 0.01 and incubated for 4 days at 37 ºC, virus titre was determined by plaque assay in SW13 cells. The virus titre was determined to be $4.2x10^{-7}$ PFU/mL.
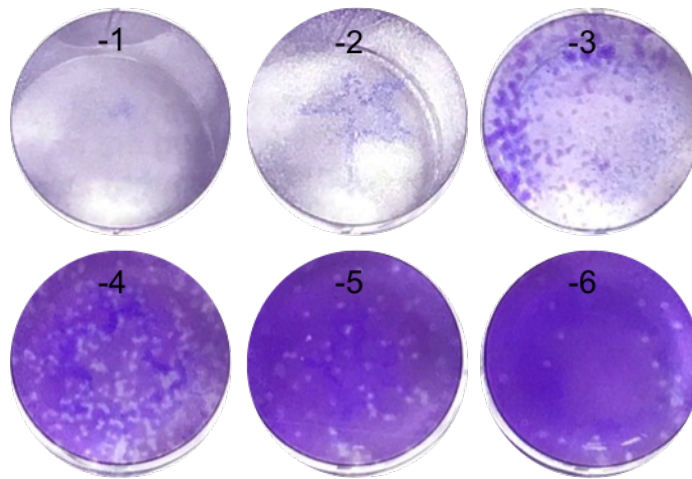
Figure 3.1: Plaque assay of BUNV.
SW13 cells were infected with a 1:100 serial dilution of BUNV (10^{-1} - 10^{-6}). Plaques were visualised using crystal violet staining. Virus titre was determined: $4.2x10^{-7}$ PFU/mL.

3.2   Time Course of BUNV

In order to determine which cell line and time point to use for the intended immuno-precipitation assays and immunofluorescence analysis, a time course was carried out

across SW13, BHK-21 and A549 cell lines. This is the first time a comparitive analysis of BUNV growth in these three cell lines has been performed. These three cell lines were chosen as SW13 cells are used to plaque BUNV, A549 cells are used for BUNV propagation and previous group members have used BHK-21 cells for BUNV propagation. Cells were infected with BUNV at an moi of 0.1 and harvested at regular intervals between 12 and 72 hpi. The expression of BUNV N is a marker for virus replication, therefore lysates were analysed by Western blot and expression of N was detected using anti-BUNV N antisera.
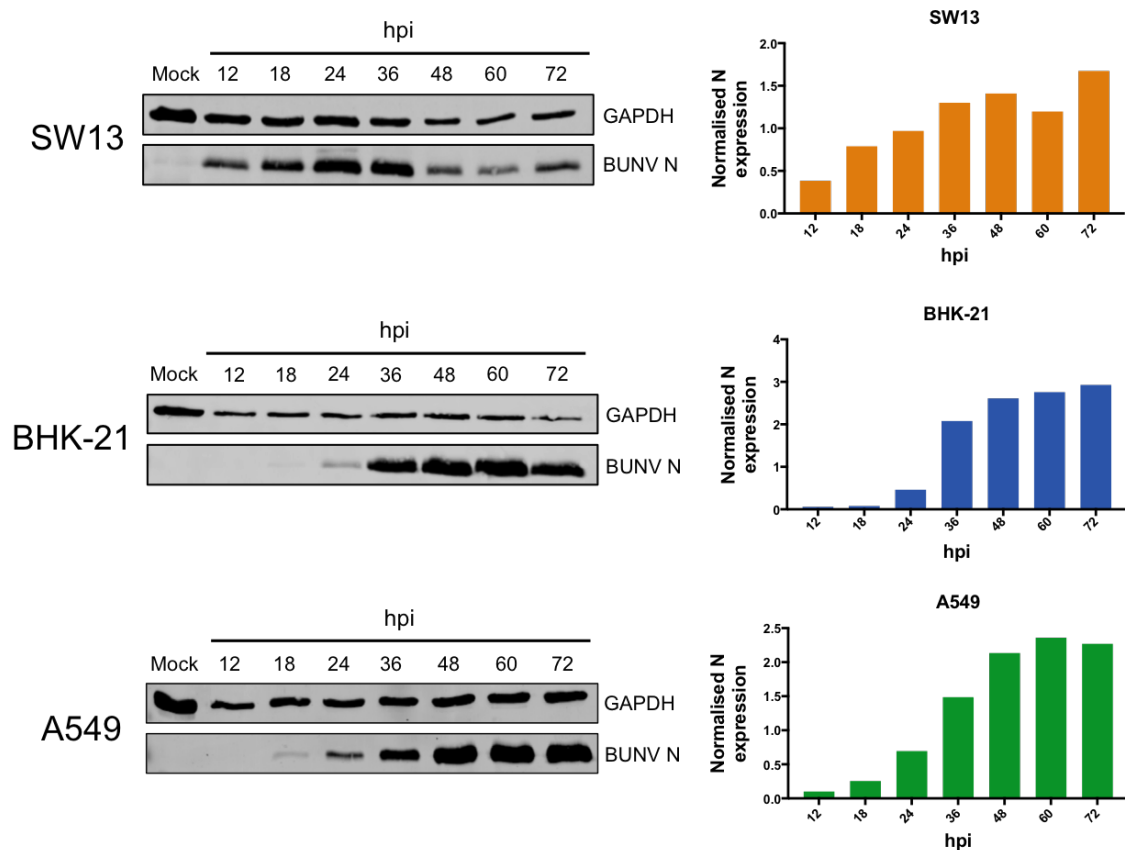
Figure 3.2: 72 hour time course of BUNV in A549, SW13 and BHK-21 cell lines. Cells were infected at an moi = 0.1 and harvested at the given time point (n=3). Lysates were analysed by Western blot and probed using primary anti-GAPDH and anti-BUNV N antibodies. The densitometry of BUNV N was calculated and normalised to the GAPDH at the given time point for the 3 repeats. These were averaged and plotted on a graph.

As seen in figure 3.2 the expression of N increased over initial time points in all three cell lines. BUNV initiates replication earlier in SW13 cells, indicated by

expression of N at 12 hpi, whereas expression of N was first detected at 18 and 24 hpi in A549 and BHK-21 cells, respectively. The expression of N continued to increase from 12 to 72 hpi in A549 cells, whereas increase of N within SW13 stopped at 36 hpi, indicating that the virus was no longer amplifying after this time point. It is also notable that from Western blot analysis, N was expressed to a higher level within A549 cells compared to SW13 cells. Cell death occured in SW13 cells, resulting in a decrease of GAPDH at 48 hpi, with similar effects detectable by 72 hpi in BHK-21 cells. Visualisation of the cells prior to harvesting revealed that following 36 hpi many SW13 and BHK-21 cells were detached (data not shown), whereas the vast majority of A549 cells remained adhered throughout the whole 72 hours. Although the normalised expression of N was high in SW13 and BHK-21 cells, the total N yield, virus yield and number of infected cells was low due to extensive cell death. Therefore, A549 cells were selected for subsequent experiments. Expression of N is was not significantly changed following 48 hpi, thus this time point was selected for subsequent analysis into interactions between N and host cell proteins.

3.3 Immunoprecipitation of the N Protein

3.3.1 Mass Spectrometry Analysis

Immunoprecipitation assays were used to identify cellular proteins interacting with BUNV N during the virus life cycle. An immunoprecipitation procedure was performed using an anti-BUNV N antibody bound to Protein G coupled Dynabeads to isolate BUNV N from infected and mock-infected A549 cells at 48 hpi. Samples from each fraction were seperated by SDS-PAGE and visualised by silver stain to determine whether host cell proteins co-immunoprecipitated with BUNV N. The presence of bands at 25 kDa and 50 kDa in both the viral- and mock-infected silver stains represent the heavy and light chains of the anti-BUNV N antibody that was bound to the Dynabeads. The presence of several bands in the elution lane of viral-infected cells, that were undetectable in mock-infected cells, indicates that

the co-immunoprecipitation was successful and suggests that BUNV N interacts with multiple cellular proteins (figure 3.3). In particular, there were three bands present in high abundance ($\approx$ 45 kDa, $\approx$ 75 kDa and $\approx$ 190 kDa), suggesting there is a strong interaction between them and BUNV N. To elucidate the identity of all cellular proteins eluted with BUNV N, the total elution fractions corresponding to the immunoprecipitations were analysed by mass spectrometry.
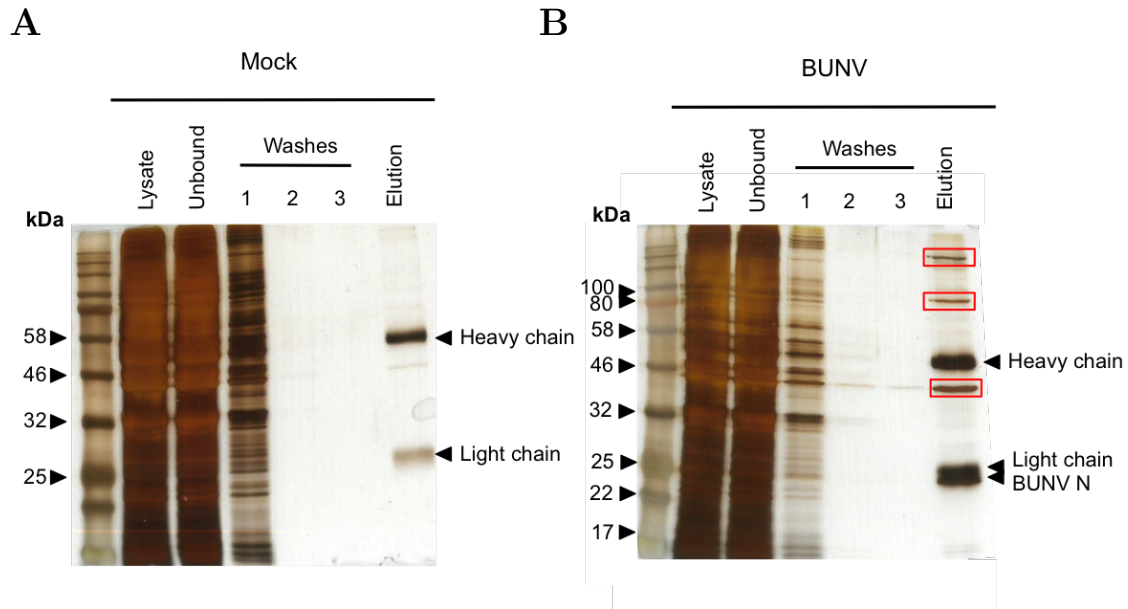
Figure 3.3: Immunoprecipitation assays analysed by silver stain
Anti-BUNV N was used to IP BUNV N from (A) mock-infected and (B) BUNV-infected A549 cells, using Protein G coupled Dynabeads. Samples from each fraction were analysed by silver stain to identify proteins that were co-immunoprecipitated with BUNV N.

The mass spectrometry data set identified approximately 200 host cell proteins (appendix) that were potential interacting partners with BUNV N. Proteins with a unique peptide count less than 3 were disregarded to eliminate false hits, creating a short list of 48 proteins. The majority of these 48 proteins are associated with the cytoskeleton and the string interaction map in figure 3.4B shows that over a quarter of these proteins are known to interact with one another. The presence of the viral RdRp, known to readily interact with N[27], verified a successful co-immunoprecipitation assay. It was notable that over a quarter of all proteins identified by mass spectrometry were cytoskeletal proteins or associated with the

cytoskeleton (e.g. proteins of the myosin family) or involved with cell-cell adhesion
(e.g. tight junction proteins).
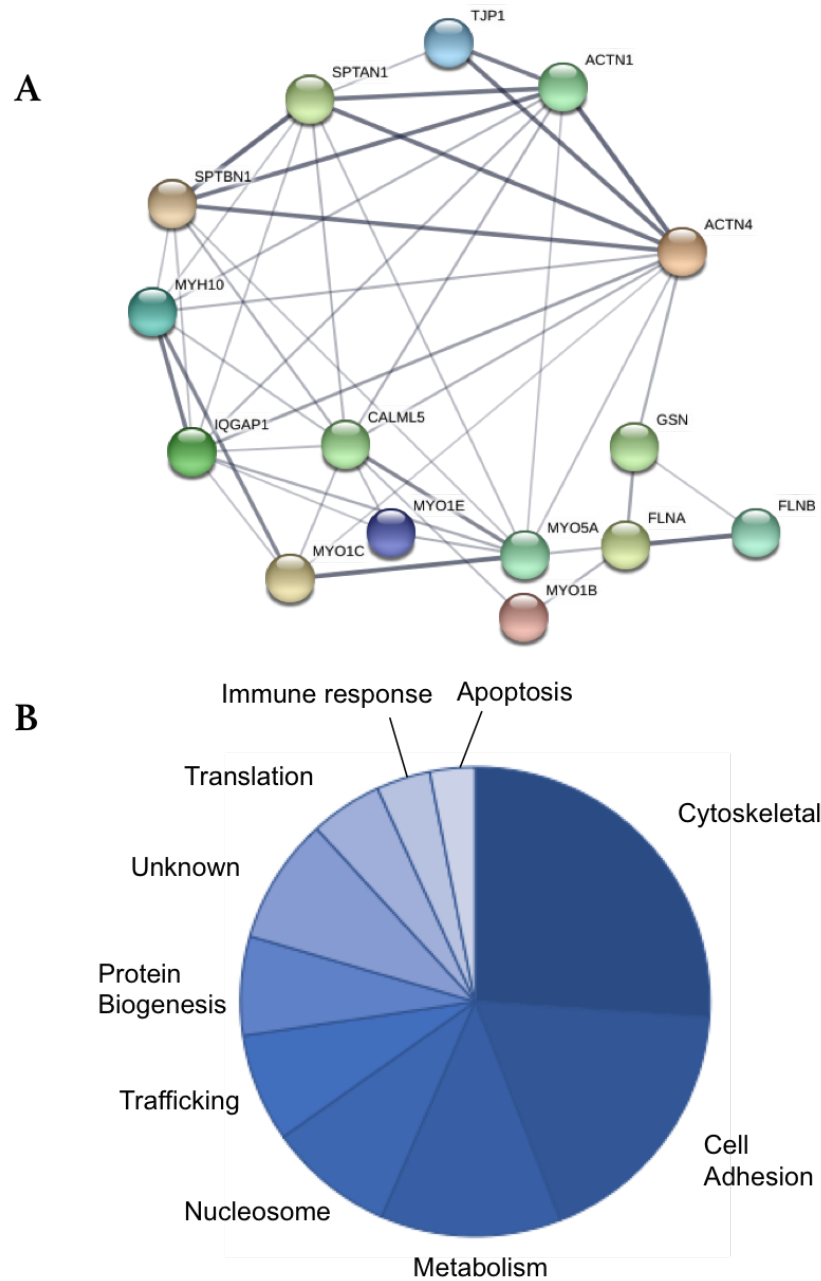
Figure 3.4: Mass spectrometry results.
(**A**) String interaction map of proteins (gene names shown) with a unique number greater
than 3, known to interact with one another within the data set. (**C**) Functional groups of
all proteins present in the mass spectrometry data set, with segment area corresponding
to the number of proteins identified in each group.

Accession	Peptides	Unique	Coverage (%)	Description
L_BUNYW	45	45	20	BUNV RdRp
NCAP_BUNYW	14	14	48	BUNV N
ACTN4_HUMAN	25	4	25	Alpha-actinin-1
HSP76_HUMAN	3	1	5	HSP70 Protein 6

Table 3.1: Mass spectrometry hits
A table to show a selection of hits from the mass spectrometry data set. The accession code can be used to find the protein on the UniProt database. The highlighted row shows the protein that was further validated. A full table of proteins can be seen in the appendix.

3.3.2 Immunoprecipitation of HAZV N

In order to justify the methodologies used to verify interactions between cellular proteins and BUNV N, co-immunoprecipitation assays were first performed with HAZV based on previous work by Surtees *et al.* (2016), to act as a positive control and confirm the immunoprecipitation validation protocol was performed correctly. By immunoprecipitation assays and Western blot analysis, Surtees *et al.* showed that the nucleocapsid protein of HAZV and CCHFV interacts with HSP70. Furthermore, by reducing the level of active HSP70 within cells using small-molecule inhibitors, virus titres were significantly decreased, proving that this interaction has a functional role during replication. The presence of HAZV N and HSP70 in the elution from virus-infected cells (figure 3.5, lane 12), and the absence of both proteins in the elution from mock-infected cells (figure 3.5, lane 6) (figure 3.5), confirms the interaction of HAZV N and HSP70, thus indicating this protocol was suitable to verify novel interacting partners.

Anti-HAZV N
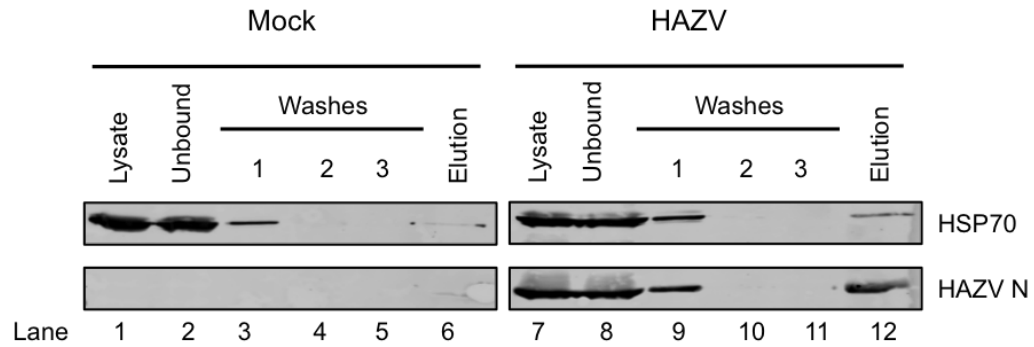
Figure 3.5: Co-immunoprecipitation of HSP70 with HAZV N.
Anti-HAZV N was used to IP HAZV N from infected or mock-infected SW13 cells, using Protein G coupled Dynabeads. HSP70 was detected using an anti-HSP70 antibody, HAZV N was detected using anti-HAZV N antisera. HSP70 was successfully co-immunoprecipitated with HAZV N as seen in the elution lane of the infected cells, but is present in the mock-infected cells to a lesser extent.

3.3.3 BUNV N and HSP70

In order to determine the identification of the band present at $\approx$ 75 kDa on the silver stain (figure 3.3), the samples from an immunoprecipitation assay were analysed by Western blot. It has been shown that N from members of two families across the bunyavirales (CCHFV, HAZV, HTNV) interacts with HSP70, which was a molecular weight of 70-71 kDa, and so could represent the $\approx$ 75 kDa band seen in figure 3.3B. The interaction between BUNV N and HSP70 within A549 cells, harvested at 48 hpi (as determined in section 3.2), was investigated by immunoprecipitation assays using Protein G coupled Dynabeads bound to anti-BUNV N antisera. The secondary antibody used during Western blotting is able to detect the heavy and light chains of the anti-BUNV N antibody eluted from the Dynabeads, as mentioned in section 3.3.1. Therefore, a smear is seen in both the viral- and mock-infected elutions at $\approx$ 25 kDa (figures 3.6 and 3.7, lanes 6 and 12. Figures 3.9 and 3.10, lanes 7 and 14).

The presence of BUNV N in the elution of infected cells (figure 3.6, lane 12, bottom panel) indicated that the immunoprecipitation was successful. However, HSP70 was absent in the infected cell elution sample (figure 3.6, lane 12, top panel)

indicating that HSP70 and BUNV N do not interact within A549 cells at 48 hpi.

Figure 3.6: Co-immunoprecipitation of HSP70 with BUNV N.
Anti-BUNV N was used to IP BUNV N from infected or mock-infected A549 cells, using Protein G coupled Dynabeads. HSP70 was detected using an anti-HSP70 antibody, BUNV N was detected using anti-BUNV N antisera. HSP70 was not successfully co-IP'd with BUNV N as there is no band present in the elution lane (lane 12) of the infected cells.

3.3.4 BUNV N and PABP

Previous studies have characterised an interaction between BUNV N and PABP that is beneficial to the viral life cycle. Through its interaction with PABP, BUNV N is able to inhibit the translation of host cell mRNAs, resulting in host cell protein synthesis shut-off. BUNV NSs protein was also shown to be important in host cell protein synthesis shut-off, however, it was not essential and PABP was still redistributed to the nucleus during infection with viruses that were deficient of NSs. As PABP is ≈ 70 kDa, further immunoprecipitaitons were performed and analysed by Western blot to determine whether PABP was the protein identity of the ≈ 75 kDa band present in figure 3.3. Similarly to the results of HSP70, BUNV N was successfully immunoprecipitated (figure 3.7, lane 12, bottom panel), however, the absence of PABP in the infected elution lane (figure 3.7, lane 12), indicated that BUNV N and PABP do not interact in A549 cells at 48 hpi.

Anti-BUNV N
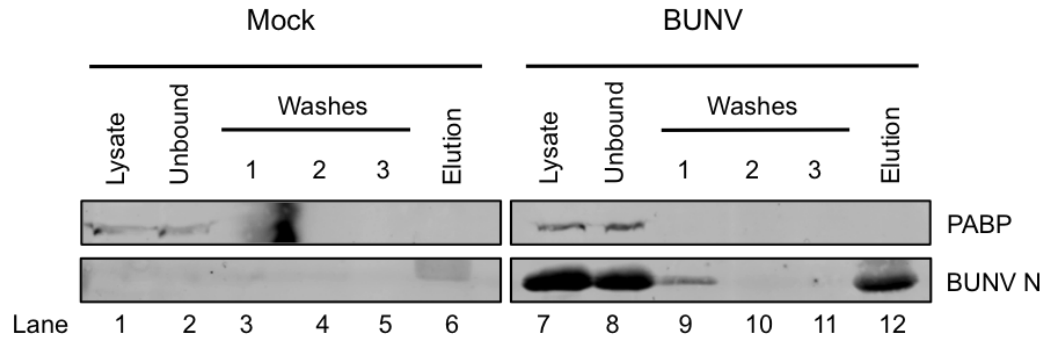
Figure 3.7: Co-immunoprecipitation of PABP with BUNV N.
Anti-BUNV N was used to IP BUNV N from infected or mock-infected A549 cells, using Protein G coupled Dynabeads. PABP was detected using an anti-PABP antibody, BUNV N was detected using anti-BUNV N antisera. PABP was not successfully co-immunoprecipitated with BUNV N as there is no band present in the elution lane (lane 12) of the infected cells.

3.3.5 Protein ID

The results of the previous sections showed N binds to various cell factors, although Western blotting with antibodies for likely cellular candidate, HSP70 and PABP, failed to conclusively show an interaction with BUNV N.

To further elucidate the identities of the three most abundant cellular proteins seen in the silver stain (figure 3.3), InstantBlue staining was used to visualise the proteins, as this stain is compatible with mass spectrometry. This staining technique is less sensitive than silver staining and only the lower two proteins ($\approx$ 45 kDa and $\approx$ 75 kDa) were able to be confidently visualised and excised from the gel to determine their protein identity. The results determined that the largest protein ($\approx$ 75 kDa) was α-actinin-4 (ACTN4) and that the smaller protein ($\approx$ 45 kDa) was actin. ACTN4 was also identified as a hit within the mass spectrometry data set (a unique peptide score of 4 and 25 % coverage (table 3.1)), therefore further analysis was undertaken to verify whether this was a robust interacting partner of BUNV N. It has been previously shown that actin is a critical support protein of the viral

tubes assembled during virus replication[29] but a direct interaction between BUNV N and actin has yet to be characterised, therefore, further analysis was carried out to investigate this potential interaction. The high abundance of both of these bands in the silver stain of the virus-infected immunoprecipitation assay samples (figure 3.3B) and their absence in the mock-infected samples (figure 3.3A), coupled with their identification through band excision and mass spectrometry analysis, indicated that these proteins were likely robust interacting partners of BUNV N.
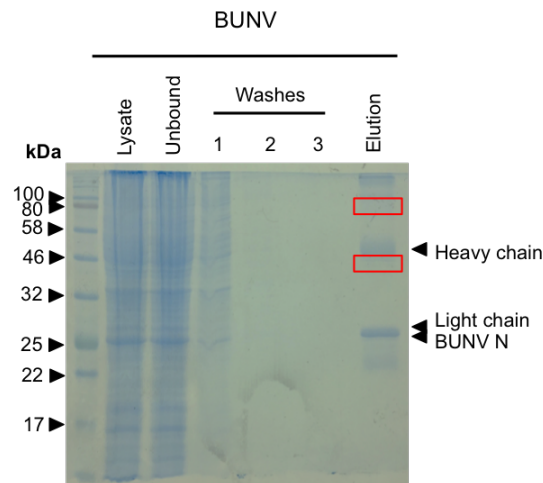
Figure 3.8: Immunoprecipitation samples visualised by InstantBlue staining Immunoprecipitation samples were visualised by InstantBlue staining in order to excise the bands highlighted in red to determine the protein identity.

3.4 Validation of Interacting Partners

3.4.1 BUNV N and Actin

It is known that actin is important in the biogenesis and maintenance of viral tube structures that are required for efficient BUNV replication[29]. It has been previously shown that actin directly interacts with nucleocapsid proteins from other members of the *Bunyavirales* in order to assemble nascent CCHFV virions[2]. As mentioned actin was identified as a potential interacting partner of BUNV N through mass spectrometry protein ID.

In order to validate the interaction between BUNV N and actin specifically, further immunoprecipitations were performed and analysed by Western blotting. The presence of BUNV N in the elution lane of infected cells (lane 14, figure 3.9A), indicated that the immunoprecipitation was successful. Actin was co-immunoprecipitated along with BUNV N, as seen in the elution lane of infected cells (figure 3.9A, lane 14). However, actin was also present in the elution of mock-infected cells (figure 3.9A, lane 7). The presence of actin in higher abundance in the mock-infected elution indicated that actin does not directly interact with BUNV N and instead suggested that actin was binding non-specifically to either the beads, protein G or the microfuge tube during the immunoprecipitation protocol. A control immunoprecipitation assay was performed using an irrelevant IgG, anti-GAPDH, as recommended by the Dynabeads protocol. The control immunoprecipitation was successful as there was no BUNV N eluted (figure 3.9B, lane 14). There was no actin present in either elution lanes (figure 3.9B, lanes 7 and 14), showing that actin was not binding to either the bead or Protein G.

A

B
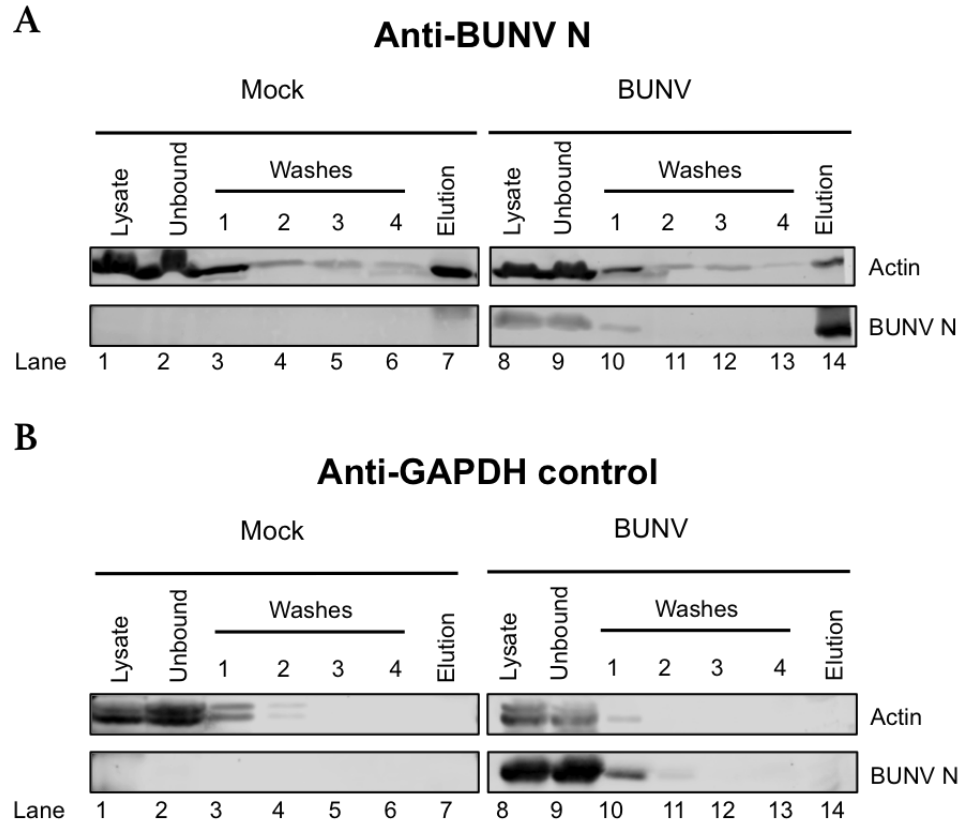
Figure 3.9: Co-immunoprecipitation of actin with BUNV N from infected and mock-infected cells.
(**A**) Anti-BUNV N was used to IP BUNV N from infected or mock-infected A549 cells, using Protein G coupled Dynabeads. Actin was detected using an anti-actin antibody, BUNV N was detected using anti-BUNV N antisera. (**B**) Control IPs were performed using anti-GAPDH bound to Protein G coupled Dynabeads.

3.4.2 BUNV N and ACTN4

ACTN4 was identified as a potential interacting partner of BUNV N through mass spectrometry protein ID analysis. ACTN4 is one of the four isoforms of α-actinin, a cytoskeletal protein that is a member of the spectrin gene superfamily[37]. ACTN4 is known to interact with the cell membrane and is involved in cell migration and adhesion. In order to validate the interaction between BUNV N and ACTN4 specifically, a further immunoprecipitation assay was performed and the samples analysed by Western blot. The immunoprecipitation was successful as BUNV N could be seen in abundance in the elution lane of virus-infected cells (figure 3.10A lane 14,

bottom panel). ACTN4 did not co-immunoprecipitate with BUNV N as it was not present in the elution lane of virus-infected cells, however, ACTN4 was present in low abundance in the mock-infected cells (figure 3.10A, lane 7, top panel). A control immunoprecipitation assay was carried out, using an irrelevant IgG (anti-GAPDH) bound to the Protein G Dynabeads. No BUNV N was immunoprecipitated as expected, however, there was a low concentration of ACTN4 in both the infected and mock-infected elution lanes (figure 3.10B, lanes 14 and 7, top panel), suggesting that ACTN4 is able to bind to either the beads or protein G.
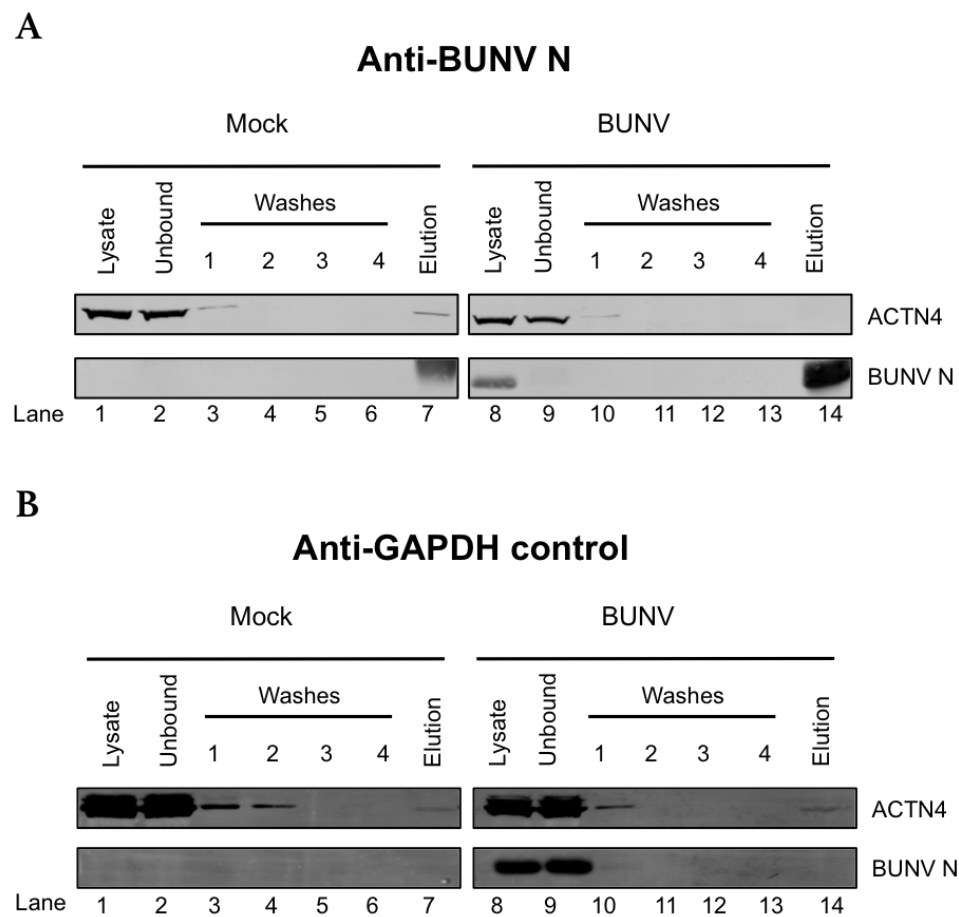
Figure 3.10: Co-immunoprecipitation of ACTN4 with BUNV N from infected and mock-infected cells.
(**A**) Anti-BUNV N was used to IP BUNV N from infected or mock-infected A549 cells, using Protein G coupled Dynabeads. ACTN4 was detected using an anti-ACTN4 antibody, BUNV N was detected using anti-BUNV N antisera.(**B**) Control IPs were performed using anti-GAPDH bound to Protein G coupled Dynabeads.

3.5   Immunofluorescence

In order to investigate the interactions between BUNV N and Actin/ACTN4 that were initially analysed by immunoprecipitations and Western blot further, confocal microscopy on immunofluorescently labelled cells was performed. Cells were stained using antibodies against BUNV N and ACTN4, whereas actin was visualised using phalloidin conjugated to an Alexa Fluor 594 and nuclei were visualised using DAPI. Cells were fixed at 48 hpi as there was high abundance of BUNV N expression at this time point, and at an moi = 0.1 the presence of both infected and uninfected cells was expected. BUNV N localised throughout the cytoplasm in intensely stained punctate regions, with a perinuclear localisation but excluded from the nucleus, consistent with previous studies. The majority of ACTN4 co-localised with actin at the cell periphery, which was expected as ACTN4 is a known binding partner of actin. Supporting the immunoprecipitation results, ACTN4 and actin were not seen to co-localise with BUNV N.
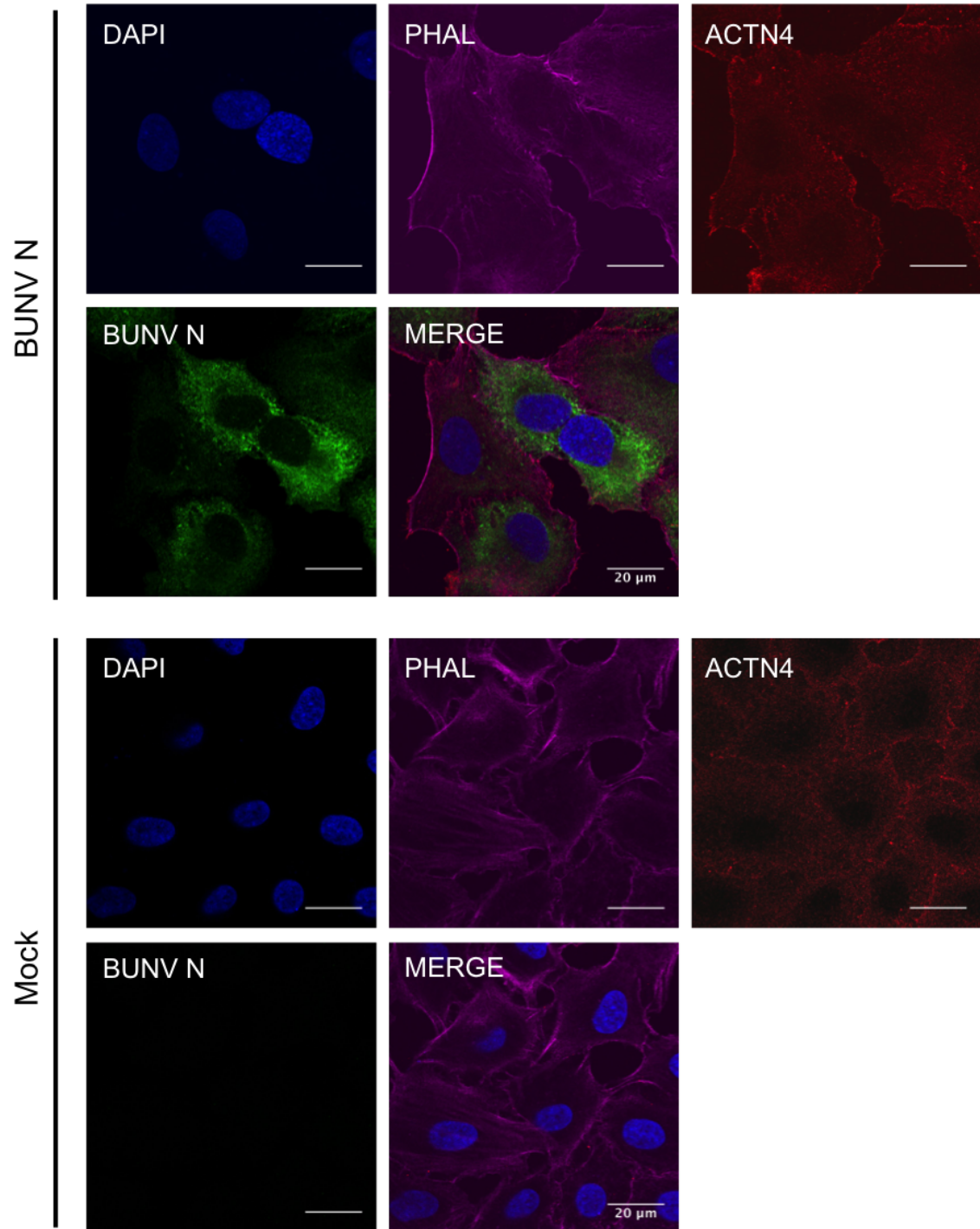
Figure 3.11: Immunofluorescence of BUNV, actin and ACTN4.
Immunofluorescence analysis of the localisation of BUNV N (green), actin (phalloidin, magenta) and ACTN4 (red) at 48 hpi. The nucleus is stained blue with DAPI.

Chapter 4

Discussion

4.1 BUNV Replication Across Cell Lines

A time course from 12-72 hpi across SW13, A549 and BHK-21 cell lines has shown that BUNV replicates at varying rates between different cell lines. These three cell lines were chosen originally as they have all previously been used in the analysis of the virus life cycle, from propagation to determining virus titre. A549 cells were the chosen cell line of this study as cell lysis occurred in both SW13 and BHK-21 cells throughout the 72 hpi time course, whereas in contrast A549 cells showed little cytopathic effects. Whilst there was a high abundance of BUNV N production at 48 hpi in both BHK-21 and A549 cell lines, A549 cells were more favourable as they are derived from humans and therefore more physiologically relevant.

The most notable difference in BUNV N expression, and therefore replication, was between A549 and SW13 cells, which is surprising as they are both human derived cell lines unlike BHK-21 cells. SW13 cells are derived from human adrenal carcinomas, whereas A549 cells are derived from adenocarcinomic human alveolar basal epithelial cells. BUNV may be able to assemble the viral tubes essential for efficient replication at an earlier time point in SW13 cells compared to A549 cells, and hence N can be detected by Western blot 12 hpi earlier. Furthermore, the cellular proteins that BUNV requires for efficient completion of the replication cycle may be more readily available within SW13 cells, allowing BUNV N to be expressed significantly earlier.

The replication of BUNV could have also been determined by analysing the

abundance of vRNA within the cell at given time points, using RT-PCR. This would allow us to follow the change in RNA synthesis throughout the virus life cycle, and determine the peak time point of vRNA synthesis. A plaque assay from each time point would have allowed us to determine the growth curve of BUNV across the different cell lines, giving insight into the amount of infectious virus released over time. The aim of this project was to identify cellular proteins interacting with N during the virus life cycle, therefore Western blot analysis of N expression was a suitable method to determine the ideal cell line and time point.

4.2 Immunoprecipitation of BUNV N

4.2.1 Mass Spectrometry results

RNA viruses have a limited coding capacity and have therefore evolved a range of mechanisms to allow them to interact with and manipulate cellular proteins to aid in efficient replication. This project aimed to elucidate the identity of cellular proteins that interact with BUNV N. The initial immunoprecipitation of BUNV N looked very promising due to the presence of several bands in the eluate of virus-infected cells that were absent in mock-infected cells, when visualised by silver stain (figure 3.3). The mass spectrometry data set revealed almost 200 cellular proteins present in the eluate of an immunoprecipitation assay from BUNV-infected cells, that had 0 spectra in the mock eluate, any proteins that had > 0 spectra within the mock eluate were immediately disregarded to highlight the difference between samples. Proteins with a unique peptide number less than 3 were disregarded next in order to eliminate any contaminants or false hits, and to conveniently reduce the candidate cellular proteins to a manageable number.

The most abundant interacting partners of BUNV N were members of the cytoskeleton, or proteins that are known to commonly associate with the cytoskeleton, including myosin and actin interacting proteins. These results are relevant with previous research from other bunyaviruses, where actin, and its interaction with

N, has been shown to be essential for the virus life cycle[3]. Members from the HSP70 family were seen within the data set, this was expected as previous research has shown HSP70 interacts with various bunyaviruses[75,89]. However, all members of this family had a unique peptide number less than 3 and were therefore disregarded as potential interacting partners of BUNV N. An immunoprecipitation assay and Western blot analysis with an anti-HSP70 antibody confirmed HSP70 does not interact with BUNV N, thus highlighting a difference between BUNV and other bunyaviruses. There were also several proteins involved in intracellular trafficking within the data set, suggesting that the cytoskeleton, along with various cellular factors, is important in the trafficking of viral proteins and RNPs to the site of virion assembly.

4.2.2 Validation of BUNV N interacting partners

Our results showed that PABP is not an interacting partner of BUNV N, which was surprising as a previous study has shown an interaction between BUNV N and PABP through co-immunoprecipitations and went on to show that PABP is retained in the nucleus following BUNV infection[12]. Similarly to the research performed throughout this project, Blakqori *et al.* carried out a proteomic approach to identify proteins co-immunoprecipitating with BUNV N. Interestingly, PABP was identified as a hit in the mass spectrometry performed by Blakqori *et al.*, although the score is not provided. PABP was not identified as a hit in the data set we collected. Whilst their immunofluorescence analysis showed the relocalisation of PABP from the cytoplasm to the nucleus at 22 hpi, it did not show co-localisation between BUNV N and PABP. Furthermore, the cells were lysed at 12 hpi for the immunoprecipitation assay, whereas cells were fixed for immunofluorescent labelling at 4, 8 and 22 hpi. One of the major differences between our work, and that carried out by Blakqori *et al.* is the choice of cell line, Blakqori *et al.* used BHK-21 cell lines whereas we used A549. As mentioned, A549 cells were chosen for this research as they were more physiologically relevant than BHK-21 cells.

It was expected that BUNV N and HSP70 would be interacting partners, as this

cellular protein has been previously shown to interact with HAZV, CCHFV and HTNV[75,89]. It is notable that the N protein from these three viruses is ≈ 50 kDa compared to BUNV N, which has a molecular weight of 26 kDa. This diversity in size will result in a variation between protein structure, which may allow the N protein from members of *Nairoviridae* and *Hantaviridae* to interact with a range of proteins that BUNV N does not. Moreover, Surtees *et al* (2016) performed experiments in HEK293T cells (derived from embryonic kidney cells) to identify HSP70 as an interacting partner of HAZV/CCHFV N and Yu *et al* (2009) performed experiments in vero E6 cells. This difference in cell line may elucidate the reason why HSP70 is a known interaction with HAZV/CCHFV/HTNV N but not with BUNV N.

It has been shown that multilamellar structures form within cells where BUNV egress occurs on the basal surface, but not within cells where virus is released on the apical surface[66]. The morphology of these structures suggested they had functions in cell adhesion and through the disruption of actin with cytochalasin D it was proposed that extracellular actin aids in the release of nascent virions and the spread of virus to neighbouring cells. This study supported the presence of ACTN4 in the mass spectrometry data set and it's identification (alongside actin) through protein ID, increasing the liklihood that these two proteins form robust interactions with BUNV N. ACTN4 interacts with actin and has known functions within cell migration and adhesion, it is therefore possible that ACTN4 is important within the assembly of these multilamellar structures and an interaction between BUNV N, actin and ACTN4 may be essential for this process.

The importance of actin during the life cycle of BUNV has been previously shown through the investigation of viral tubes that are required for BUNV morphogenesis[29], yet an interaction between BUNV N and actin has yet to be characterised. Actin was not a hit within the mass spectrometry data set containing all proteins within the eluate, however, the band present at ≈ 45 kDa when the eluate was visualised by InstantBlue stain was identified as actin (figure 3.8). Additional analysis of the interaction between actin and BUNV N through Western blotting and immunofluorescence determined that actin does not interact with BUNV N. Impor-

tantly, BHK-21 cells were used by Fontana *et al.* (2008) during the investigation into the architecture of viral tubes, whereas the immunoprecipitation assays and immunofluorescence was performed in A549 cells during this study. As seen in section 3.2, BUNV replicates at varying rates across cell lines and it is therefore possible that the virus interacts with the cellular factors differently between cell types. Cells were lysed at 48 hpi throughout this current study, whereas the visualisation of viral factories by Fontana *et al.* was at 8 hpi. It is possible that BUNV N and actin do interact during the assembly of viral tubes and the interaction may occur much earlier than the time points we investigated during the current study. Through control immunoprecipitation assays it was confirmed that actin was not binding to either Protein G or the Dynabeads and it is therefore potentially interacting with the anti-BUNV N antibody, although there was no cross-reactivity between anti-BUNV N and actin during Western blotting. Immunoprecipitation assays could be repeated at earlier time points that are relevant to those used by Fontana *et al.* (2008), and in BHK-21 cells, in order to determine whether BUNV N interacts with actin during viral tube formation.

ACTN4 was a hit within the mass spectrometry data set and importantly it had a unique peptide number greater than 3, it was also identified as one of the three brightest bands seen within infected eluate when visualised by silver stain (figure 3.3). This correlation between both mass spectrometry analysis data indicated that ACTN4 may be a true interacting partner of BUNV N, however, further analysis by Western blotting revealed that ACTN4 may be a contaminant and was in fact binding to either the Dynabeads of Protein G (figure 3.10). This was surprising as in the initial silver stain of eluates from both viral- and mock-infected cells showed several bands that were significantly more intense within viral-infected samples than any bands present within the mock-infected samples.

4.3 Future work

If ACTN4 and actin had been identified as true interacting partners of BUNV N, further analysis could be carried out to determine the importance of this interaction for efficient virus replication. The expression of cellular proteins can be silenced using siRNA, a commonly used RNA interference tool that is able to target specific mRNA for degradation, or known specific inhibitors (e.g. cytochalasin D). Western blot analysis of the expression of N over time would allow us to compare the levels of BUNV replication in cells with silenced actin/ACTN4 in comparison with untreated cells. The level of vRNA synthesis can be analysed by rt-PCR to give further insight into BUNV replication. Moreover, plaque assays of the virus released from cells with silenced actin/ACTN4 would allow us to determine if the knockdown of cellular proteins results in a reduction of infectious virion production and release. Fontana *et al.* (2008) showed that when cells were treated with jasplakinolide (an actin-stabilising drug) infectious virus release was decreased by 60-70 % due to the displacement of cell organelles to the periphery, proving the importance of actin in maintaining the stability of viral tubes, and thus efficient virus assembly. Purifying released virus would allow us to determine whether the cellular proteins that are known interacting partners of BUNV N are incorporated into mature virions. It has already been shown that actin is present in immature virions but not fully matured extracellular virions[29].

The interaction between cellular proteins and BUNV N could be investigated further by analysing the localisation of newly synthesised vRNA, BUNV N and the cellular protein through immunofluorescently labelled cells. 5-ethynyl uridine (5-EU) is a uridine analogue that is incorporated into RNA during transcription. Actinomycin D is an antibiotic that interferes with cellular mRNA synthesis by binding DNA at the initiation complex and preventing the elongation of RNA. As this mechanism is DNA dependent it has no effect on BUNV RNA synthesis, allowing targetted labelling of nascently synthesised vRNA with 5-EU. BUNV N is expected to co-localise with vRNA synthesis as RNA is immediately encapsidated by N. If

the cellular protein also co-localises with BUNV N and 5-EU labelled vRNA, the interaction may be important for genome replication and transcription. Using a replicon system rather than live virus allows investigation into just the replication cycle of BUNV without entry/assembly/egress. The use of siRNA to knockdown cellular proteins would allow for the confirmation of the host proteins importance for virus replication.

References

[1] Adam, I. and Karsany, M. S. (2008). Case report: Rift Valley Fever with vertical transmission in a pregnant Sudanese woman. Journal of Medical Virology *80*, 929–929.

[2] Andersson, I., Bladh, L., Mousavi-Jazi, M., Magnusson, K.-E., Lundkvist, A., Haller, O. and Mirazimi, A. (2004a). Human MxA protein inhibits the replication of Crimean-Congo hemorrhagic fever virus. Journal of virology *78*, 4323–9.

[3] Andersson, I., Simon, M., Lundkvist, A., Nilsson, M., Holmström, A., Elgh, F. and Mirazimi, A. (2004b). Role of actin filaments in targeting of Crimean Congo hemorrhagic fever virus nucleocapsid protein to perinuclear regions of mammalian cells. Journal of Medical Virology *72*, 83–93.

[4] Ariza, A., Tanner, S. J., Walter, C. T., Dent, K. C., Shepherd, D. A., Wu, W., Matthews, S. V., Hiscox, J. A., Green, T. J., Luo, M., Elliott, R. M., Fooks, A. R., Ashcroft, A. E., Stonehouse, N. J., Ranson, N. A., Barr, J. N. and Edwards, T. A. (2013). Nucleocapsid protein structures from orthobunyaviruses reveal insight into ribonucleoprotein architecture and RNA polymerization. Nucleic Acids Research *41*, 5912–5926.

[5] Barr, J. N. (2007). Bunyavirus mRNA synthesis is coupled to translation to prevent premature transcription termination. RNA (New York, N.Y.) *13*, 731–6.

[6] Barr, J. N., Elliott, R. M., Dunn, E. F. and Wertz, G. W. (2003). Segment-specific terminal sequences of Bunyamwera bunyavirus regulate genome replication. Virology *311*, 326–38.

[7] Barr, J. N., Rodgers, J. W. and Wertz, G. W. (2005). The Bunyamwera Virus mRNA Transcription Signal Resides within both the 3' and the 5' Terminal Regions and Allows Ambisense Transcription from a Model RNA Segment. Journal of Virology *79*, 12602–12607.

[8] Barr, J. N. and Wertz, G. W. (2004). Bunyamwera bunyavirus RNA synthesis requires cooperation of 3'- and 5'-terminal sequences. Journal of virology *78*, 1129–38.

[9] Barr, J. N. and Wertz, G. W. (2005). Role of the conserved nucleotide mismatch within 3'- and 5'-terminal regions of Bunyamwera virus in signaling transcription. Journal of virology *79*, 3586–94.

[10] Battisti, A. J., Chu, Y.-K., Chipman, P. R., Kaufmann, B., Jonsson, C. B. and Rossmann, M. G. (2011). Structural Studies of Hantaan Virus. Journal of Virology *85*, 835–841.

[11] Blair, C. and Olson, K. (2015). The Role of RNA Interference (RNAi) in Arbovirus-Vector Interactions. Viruses *7*, 820–843.

[12] Blakqori, G., van Knippenberg, I. and Elliott, R. M. (2009). Bunyamwera Orthobunyavirus S-Segment Untranslated Regions Mediate Poly(A) Tail-Independent Translation. Journal of Virology *83*, 3637–3646.

[13] Blakqori, G. and Weber, F. (2005). Efficient cDNA-based rescue of La Crosse bunyaviruses expressing or lacking the nonstructural protein NSs. Journal of virology *79*, 10420–8.

[14] Bowen, M. D., Trappier, S. G., Sanchez, A. J., Meyer, R. F., Goldsmith, C. S., Zaki, S. R., Dunster, L. M., Peters, C., Ksiazek, T. G., Nichol, S. T. and RVF Task Force (2001). A Reassortant Bunyavirus Isolated from Acute Hemorrhagic Fever Cases in Kenya and Somalia. Virology *291*, 185–190.

[15] Bricio-Moreno, L., Sheridan, V. H., Goodhead, I., Armstrong, S., Wong, J. K., Waters, E. M., Sarsby, J., Panagiotou, S., Dunn, J., Chakraborty, A., Fang, Y., Griswold, K. E., Winstanley, C., Fothergill, J. L., Kadioglu, A. and Neill, D. R. (2018). Evolutionary trade-offs associated with loss of PmrB function in host-adapted Pseudomonas aeruginosa. Nature Communications *9*, 2635.

[16] Bridgen, A., Weber, F., Fazakerley, J. K. and Elliott, R. M. (2001). Bunyamwera bunyavirus nonstructural protein NSs is a nonessential gene product that contributes to viral pathogenesis. Proceedings of the National Academy of Sciences of the United States of America *98*, 664–9.

[17] Briese, T., Bird, B., Kapoor, V., Nichol, S. T. and Lipkin, W. I. (2006). Batai and Ngari viruses: M segment reassortment and association with severe febrile disease outbreaks in East Africa. Journal of virology *80*, 5627–30.

[18] Carter, S. D., Surtees, R., Walter, C. T., Ariza, A., Bergeron, E., Nichol, S. T., Hiscox, J. A., Edwards, T. A. and Barr, J. N. (2012). Structure, function, and evolution of the Crimean-Congo hemorrhagic fever virus nucleocapsid protein. Journal of virology *86*, 10914–23.

[19] Couturier, M., Buccellato, M., Costanzo, S., Bourhis, J.-M., Shu, Y., Nicaise, M., Desmadril, M., Flaudrops, C., Longhi, S. and Oglesbee, M. (2009). High affinity binding between Hsp70 and the C-terminal domain of the measles virus nucleoprotein requires an Hsp40 co-chaperone. Journal of Molecular Recognition *23*, n/a–n/a.

[20] Dessau, M. and Modis, Y. (2013). Crystal structure of glycoprotein C from Rift Valley fever virus. Proceedings of the National Academy of Sciences *110*, 1696–1701.

[21] Dietrich, I., Shi, X., McFarlane, M., Watson, M., Blomström, A.-L., Skelton, J. K., Kohl, A., Elliott, R. M. and Schnettler, E. (2017). The Antiviral RNAi Response in Vector and Non-vector Cells against Orthobunyaviruses. PLOS Neglected Tropical Diseases *11*, e0005272.

[22] Dong, H., Li, P., Elliott, R. M. and Dong, C. (2013). Structure of Schmallenberg orthobunyavirus nucleoprotein suggests a novel mechanism of genome encapsidation. Journal of virology *87*, 5593–601.

[23] Duh, D., Nichol, S. T., Khristova, M. L., Saksida, A., Hafner-Bratkovic, I., Petrovec, M., Dedushaj, I., Ahmeti, S. and Avsic-Zupanc, T. (2008). The complete genome sequence of a Crimean-Congo hemorrhagic fever virus isolated from an endemic region in Kosovo. Virology journal *5*, 7.

[24] Dutuze, M. F., Nzayirambaho, M., Mores, C. N. and Christofferson, R. C. (2018). A Review of Bunyamwera, Batai, and Ngari Viruses: Understudied Orthobunyaviruses With Potential One Health Implications. Frontiers in veterinary science *5*, 69.

[25] Eifan, S., Schnettler, E., Dietrich, I., Kohl, A. and Blomström, A.-L. (2013). Non-Structural Proteins of Arthropod-Borne Bunyaviruses: Roles and Functions. Viruses *5*, 2447–2468.

[26] Eifan, S. A. and Elliott, R. M. (2009). Mutational analysis of the Bunyamwera orthobunyavirus nucleocapsid protein gene. Journal of virology *83*, 11307–17.

[27] Elliott, R. M. (2014). Orthobunyaviruses: recent genetic and structural insights. Nature Reviews Microbiology *12*, 673–685.

[28] European Food Safety Authority (2013). "Schmallenberg" virus: analysis of the epidemiological data (May 2013). EFSA Supporting Publications *10*.

[29] Fontana, J., López-Montero, N., Elliott, R. M., Fernández, J. J. and Risco, C. (2008). The unique architecture of Bunyamwera virus factories around the Golgi complex. Cellular Microbiology *10*, 2012–2028.

[30] Garcin, D., Lezzi, M., Dobbs, M., Elliott, R. M., Schmaljohn, C., Kang, C. Y. and Kolakofsky, D. (1995). The 5' ends of Hantaan virus (Bunyaviridae) RNAs suggest a prime-and-realign mechanism for the initiation of RNA synthesis. Journal of virology *69*, 5754–62.

[31] Garry, C. E. and Garry, R. F. (2004). Proteomics computational analyses suggest that the carboxyl terminal glycoproteins of Bunyaviruses are class II viral fusion protein (beta-penetrenes). Theoretical Biology and Medical Modelling *1*, 10.

[32] Gerlach, P., Malet, H., Cusack, S. and Reguera, J. (2015). Structural Insights into Bunyavirus Replication and Its Regulation by the vRNA Promoter. Cell *161*, 1267–1279.

[33] Haque, A. and Mir, M. A. (2010). Interaction of hantavirus nucleocapsid protein with ribosomal protein S19. Journal of virology *84*, 12450–3.

[34] Hart, T. J., Kohl, A. and Elliott, R. M. (2009). Role of the NSs Protein in the Zoonotic Capacity of Orthobunyaviruses. Zoonoses and Public Health *56*, 285–296.

[35] Hoffmann, B., Scheuch, M., Höper, D., Jungblut, R., Holsteg, M., Schirrmeier, H., Eschbaumer, M., Goller, K. V., Wernike, K., Fischer, M., Breithaupt, A., Mettenleiter, T. C. and Beer, M. (2012). Novel Orthobunyavirus in Cattle, Europe, 2011. Emerging Infectious Diseases *18*, 469–472.

[36] Hollidge, B. S., Nedelsky, N. B., Salzano, M.-V., Fraser, J. W., Gonzalez-Scarano, F. and Soldan, S. S. (2012). Orthobunyavirus Entry into Neurons and Other Mammalian Cells Occurs via Clathrin-Mediated Endocytosis and Requires Trafficking into Early Endosomes. Journal of Virology *86*, 7988–8001.

[37] Honda, K. (2015). The biological role of actinin-4 (ACTN4) in malignant phenotypes of cancer. Cell & Bioscience *5*, 41.

[38] Jeeva, S., Cheng, E., Ganaie, S. S. and Mir, M. A. (2017). Crimean-Congo Hemorrhagic Fever Virus Nucleocapsid Protein Augments mRNA Translation. Journal of virology *91*, 00636–17.

[39] Jones, D. T., Taylor, W. R. and Thornton, J. M. (1992). The rapid generation of mutation data matrices from protein sequences. Computer applications in the biosciences : CABIOS *8*, 275–82.

[40] Kim, K.-H., Yi, J., Kim, G., Choi, S. J., Jun, K. I., Kim, N.-H., Choe, P. G., Kim, N.-J., Lee, J.-K. and Oh, M.-d. (2013). Severe Fever with Thrombocytopenia Syndrome, South Korea, 2012. Emerging Infectious Diseases *19*.

[41] Kohl, A., Clayton, R. F., Weber, F., Bridgen, A., Randall, R. E. and Elliott, R. M. (2003). Bunyamwera virus nonstructural protein NSs counteracts interferon regulatory factor 3-mediated induction of early cell death. Journal of virology *77*, 7999–8008.

[42] Kohl, A., Dunn, E. F., Lowen, A. C. and Elliott, R. M. (2004a). Complementarity, sequence and structural elements within the 3' and 5' non-coding regions of the Bunyamwera orthobunyavirus S segment determine promoter strength. Journal of General Virology *85*, 3269–3278.

[43] Kohl, A., Hart, T. J., Noonan, C., Royall, E., Roberts, L. O. and Elliott, R. M. (2004b). A Bunyamwera Virus
Minireplicon System in Mosquito Cells. Journal of Virology *78*, 5679–5685.

[44] Kumar, S., Stecher, G. and Tamura, K. (2016). MEGA7: Molecular Evolutionary Genetics Analysis Version
7.0 for Bigger Datasets. Molecular Biology and Evolution *33*, 1870–1874.

[45] Lahaye, X., Vidy, A., Fouquet, B. and Blondel, D. (2012). Hsp70 protein positively regulates rabies virus
infection. Journal of virology *86*, 4743–51.

[46] Léonard, V. H. J., Kohl, A., Hart, T. J. and Elliott, R. M. (2006). Interaction of Bunyamwera Orthobunyavirus
NSs protein with mediator protein MED8: a mechanism for inhibiting the interferon response. Journal of virology
80, 9667–75.

[47] Leonard, V. H. J., Kohl, A., Osborne, J. C., McLees, A. and Elliott, R. M. (2005). Homotypic Interaction of
Bunyamwera Virus Nucleocapsid Protein. Journal of Virology *79*, 13166–13172.

[48] Li, B., Wang, Q., Pan, X., Fernández de Castro, I., Sun, Y., Guo, Y., Tao, X., Risco, C., Sui, S.-F. and
Lou, Z. (2013). Bunyamwera virus possesses a distinct nucleocapsid protein to facilitate genome encapsidation.
Proceedings of the National Academy of Sciences of the United States of America *110*, 9048–53.

[49] Li, C.-X., Shi, M., Tian, J.-H., Lin, X.-D., Kang, Y.-J., Chen, L.-J., Qin, X.-C., Xu, J., Holmes, E. C. and
Zhang, Y.-Z. (2015). Unprecedented genomic diversity of RNA viruses in arthropods reveals the ancestry of
negative-sense RNA viruses. eLife *4*.

[50] Li, X.-D., Lankinen, H., Vaheri, A., Koistinen, V., Soliymani, R., Vapalahti, O., Guo, D. and Mäkelä, T. P.
(2002). Hantavirus nucleocapsid protein interacts with the Fas-mediated apoptosis enhancer Daxx. Journal of
General Virology *83*, 759–766.

[51] Li, Z., Hu, J., Bao, C., Li, P., Qi, X., Qin, Y., Wang, S., Tan, Z., Zhu, Y., Tang, F. and Zhou, M. (2014).
Seroprevalence of antibodies against SFTS virus infection in farmers and animals, Jiangsu, China. Journal of
Clinical Virology *60*, 185–189.

[52] López-Montero, N. and Risco, C. (2011). Self-protection and survival of arbovirus-infected mosquito cells.
Cellular Microbiology *13*, 300–315.

[53] Lowen, A. C. and Elliott, R. M. (2005). Mutational analyses of the nonconserved sequences in the Bunyamwera
Orthobunyavirus S segment untranslated regions. Journal of virology *79*, 12861–70.

[54] Maes, P., Alkhovsky, S. V., Bào, Y., Beer, M., Birkhead, M., Briese, T., Buchmeier, M. J., Calisher, C. H.,
Charrel, R. N., Choi, I. R., Clegg, C. S., de la Torre, J. C., Delwart, E., DeRisi, J. L., Di Bello, P. L., Di Serio,
F., Digiaro, M., Dolja, V. V., Drosten, C., Druciarek, T. Z., Du, J., Ebihara, H., Elbeaino, T., Gergerich, R. C.,
Gillis, A. N., Gonzalez, J.-P. J., Haenni, A.-L., Hepojoki, J., Hetzel, U., Ho, T., Hóng, N., Jain, R. K., Jansen van
Vuren, P., Jin, Q., Jonson, M. G., Junglen, S., Keller, K. E., Kemp, A., Kipar, A., Kondov, N. O., Koonin, E. V.,
Kormelink, R., Korzyukov, Y., Krupovic, M., Lambert, A. J., Laney, A. G., LeBreton, M., Lukashevich, I. S.,
Marklewitz, M., Markotter, W., Martelli, G. P., Martin, R. R., Mielke-Ehret, N., Mühlbach, H.-P., Navarro, B.,
Ng, T. F. F., Nunes, M. R. T., Palacios, G., Pawęska, J. T., Peters, C. J., Plyusnin, A., Radoshitzky, S. R.,
Romanowski, V., Salmenperä, P., Salvato, M. S., Sanfaçon, H., Sasaya, T., Schmaljohn, C., Schneider, B. S.,
Shirako, Y., Siddell, S., Sironen, T. A., Stenglein, M. D., Storm, N., Sudini, H., Tesh, R. B., Tzanetakis, I. E.,
Uppala, M., Vapalahti, O., Vasilakis, N., Walker, P. J., Wáng, G., Wáng, L., Wáng, Y., Wèi, T., Wiley, M. R.,

Wolf, Y. I., Wolfe, N. D., Wú, Z., Xú, W., Yang, L., Yāng, Z., Yeh, S.-D., Zhāng, Y.-Z., Zhèng, Y., Zhou, X., Zhū, C., Zirkel, F. and Kuhn, J. H. (2018). Taxonomy of the family Arenaviridae and the order Bunyavirales: update 2018. Archives of Virology *163*, 2295–2310.

[55] Manigold, T. and Vial, P. (2014). Human hantavirus infections: epidemiology, clinical features, pathogenesis and immunology. Swiss Medical Weekly *144*, w13937.

[56] Mohl, B.-P. and Barr, J. N. (2009). Investigating the specificity and stoichiometry of RNA binding by the nucleocapsid protein of Bunyamwera virus. RNA (New York, N.Y.) *15*, 391–9.

[57] Novoa, R. R., Calderita, G., Cabezas, P., Elliott, R. M. and Risco, C. (2005). Key Golgi factors for structural and functional maturation of bunyamwera virus. Journal of virology *79*, 10852–63.

[58] Pappu, H., Jones, R. and Jain, R. (2009). Global status of tospovirus epidemics in diverse cropping systems: Successes achieved and challenges ahead. Virus Research *141*, 219–236.

[59] Park, S.-W., Han, M.-G., Yun, S.-M., Park, C., Lee, W.-J. and Ryou, J. (2014). Severe Fever with Thrombocytopenia Syndrome Virus, South Korea, 2013. Emerging Infectious Diseases *20*, 1880–1882.

[60] Plassmeyer, M. L., Soldan, S. S., Stachelek, K. M., Roth, S. M., Martín-García, J. and González-Scarano, F. (2007). Mutagenesis of the La Crosse Virus glycoprotein supports a role for Gc (1066–1087) as the fusion peptide. Virology *358*, 273–282.

[61] Raymond, D. D., Piper, M. E., Gerrard, S. R., Skiniotis, G. and Smith, J. L. (2012). Phleboviruses encapsidate their genomes by sequestering RNA bases. Proceedings of the National Academy of Sciences *109*, 19208–19213.

[62] Reguera, J., Malet, H., Weber, F. and Cusack, S. (2013). Structural basis for encapsidation of genomic RNA by La Crosse Orthobunyavirus nucleoprotein. Proceedings of the National Academy of Sciences of the United States of America *110*, 7246–51.

[63] Reguera, J., Weber, F. and Cusack, S. (2010). Bunyaviridae RNA Polymerases (L-Protein) Have an N-Terminal, Influenza-Like Endonuclease Domain, Essential for Viral Cap-Dependent Transcription. PLoS Pathogens *6*, e1001101.

[64] Salanueva, I. J., Novoa, R. R., Cabezas, P., López-Iglesias, C., Carrascosa, J. L., Elliott, R. M. and Risco, C. (2003). Polymorphism and structural maturation of bunyamwera virus in Golgi and post-Golgi compartments. Journal of virology *77*, 1368–81.

[65] Santos, R. I., Rodrigues, A. H., Silva, M. L., Mortara, R. A., Rossi, M. A., Jamur, M. C., Oliver, C. and Arruda, E. (2008). Oropouche virus entry into HeLa cells involves clathrin and requires endosomal acidification. Virus Research *138*, 139–143.

[66] Sanz-Sánchez, L. and Risco, C. (2013). Multilamellar structures and filament bundles are found on the cell surface during bunyavirus egress. PloS one *8*, e65526.

[67] Schlecht, R., Scholz, S. R., Dahmen, H., Wegener, A., Sirrenberg, C., Musil, D., Bomke, J., Eggenweiler, H.-M., Mayer, M. P. and Bukau, B. (2013). Functional Analysis of Hsp70 Inhibitors. PLoS ONE *8*, e78443.

[68] Shayan, S., Bokaean, M., Shahrivar, M. R. and Chinikar, S. (2015). Crimean-Congo Hemorrhagic Fever. Laboratory Medicine *46*, 180–189.

[69] Shi, X., Goli, J., Clark, G., Brauburger, K. and Elliott, R. M. (2009). Functional analysis of the Bunyamwera orthobunyavirus Gc glycoprotein. The Journal of general virology *90*, 2483–92.

[70] Shi, X., Kohl, A., Léonard, V. H. J., Li, P., McLees, A. and Elliott, R. M. (2006). Requirement of the N-terminal region of orthobunyavirus nonstructural protein NSm for virus assembly and morphogenesis. Journal of virology *80*, 8089–99.

[71] Shi, X., Kohl, A., Li, P. and Elliott, R. M. (2007). Role of the Cytoplasmic Tail Domains of Bunyamwera Orthobunyavirus Glycoproteins Gn and Gc in Virus Assembly and Morphogenesis. Journal of Virology *81*, 10151–10160.

[72] Shi, X., Lappin, D. F. and Elliott, R. M. (2004). Mapping the Golgi Targeting and Retention Signal of Bunyamwera Virus Glycoproteins. Journal of Virology *78*, 10793–10802.

[73] Song, J.-W., Baek, L. J., Schmaljohn, C. S. and Yanagihara, R. (2007). Thottapalayam virus, a prototype shrewborne hantavirus. Emerging infectious diseases *13*, 980–5.

[74] Surtees, R., Ariza, A., Punch, E. K., Trinh, C. H., Dowall, S. D., Hewson, R., Hiscox, J. A., Barr, J. N. and Edwards, T. A. (2015). The crystal structure of the Hazara virus nucleocapsid protein. BMC Structural Biology *15*, 24.

[75] Surtees, R., Dowall, S. D., Shaw, A., Armstrong, S., Hewson, R., Carroll, M. W., Mankouri, J., Edwards, T. A., Hiscox, J. A. and Barr, J. N. (2016). Heat Shock Protein 70 Family Members Interact with Crimean-Congo Hemorrhagic Fever Virus and Hazara Virus Nucleocapsid Proteins and Perform a Functional Role in the Nairovirus Replication Cycle. Journal of Virology *90*, 9305–9316.

[76] Szemiel, A. M., Failloux, A.-B. and Elliott, R. M. (2012). Role of Bunyamwera Orthobunyavirus NSs Protein in Infection of Mosquito Cells. PLoS Neglected Tropical Diseases *6*, e1823.

[77] Takahashi, T., Maeda, K., Suzuki, T., Ishido, A., Shigeoka, T., Tominaga, T., Kamei, T., Honda, M., Ninomiya, D., Sakai, T., Senba, T., Kaneyuki, S., Sakaguchi, S., Satoh, A., Hosokawa, T., Kawabe, Y., Kurihara, S., Izumikawa, K., Kohno, S., Azuma, T., Suemori, K., Yasukawa, M., Mizutani, T., Omatsu, T., Katayama, Y., Miyahara, M., Ijuin, M., Doi, K., Okuda, M., Umeki, K., Saito, T., Fukushima, K., Nakajima, K., Yoshikawa, T., Tani, H., Fukushi, S., Fukuma, A., Ogata, M., Shimojima, M., Nakajima, N., Nagata, N., Katano, H., Fukumoto, H., Sato, Y., Hasegawa, H., Yamagishi, T., Oishi, K., Kurane, I., Morikawa, S. and Saijo, M. (2014). The First Identification and Retrospective Study of Severe Fever With Thrombocytopenia Syndrome in Japan. The Journal of Infectious Diseases *209*, 816–827.

[78] Tarlinton, R., Daly, J., Dunham, S. and Kydd, J. (2012). The challenge of Schmallenberg virus emergence in Europe. The Veterinary Journal *194*, 10–18.

[79] Taylor, S. L., Frias-Staheli, N., Garcia-Sastre, A. and Schmaljohn, C. S. (2009). Hantaan Virus Nucleocapsid Protein Binds to Importin Proteins and Inhibits Tumor Necrosis Factor Alpha-Induced Activation of Nuclear Factor Kappa B. Journal of Virology *83*, 1271–1279.

[80] Tesh, R. B. and Modi, G. B. (1987). Maintenance of Toscana virus in Phlebotomus perniciosus by vertical transmission. The American journal of tropical medicine and hygiene *36*, 189–93.

[81] Thomas, D., Blakqori, G., Wagner, V., Banholzer, M., Kessler, N., Elliott, R. M., Haller, O. and Weber, F. (2004). Inhibition of RNA Polymerase II Phosphorylation by a Viral Interferon Antagonist. Journal of Biological Chemistry *279*, 31471–31477.

[82] van Knippenberg, I., Fragkoudis, R. and Elliott, R. M. (2013). The Transient Nature of Bunyamwera Orthobunyavirus NSs Protein Expression: Effects of Increased Stability of NSs Protein on Virus Replication. PLoS ONE *8*, e64137.

[83] Walter, C. T. and Barr, J. N. (2011). Recent advances in the molecular and cellular biology of bunyaviruses. Journal of General Virology *92*, 2467–2484.

[84] Watts, D. M., Pantuwatana, S., DeFoliart, G. R., Yuill, T. M. and Thompson, W. H. (1973). Transovarial transmission of LaCrosse virus (California encephalitis group) in the mosquito, Aedes triseriatus. Science (New York, N.Y.) *182*, 1140–1.

[85] Willensky, S., Bar-Rogovsky, H., Bignon, E. A., Tischler, N. D., Modis, Y. and Dessau, M. (2016). Crystal Structure of Glycoprotein C from a Hantavirus in the Post-fusion Conformation. PLOS Pathogens *12*, e1005948.

[86] Yanase, T., Kato, T., Aizawa, M., Shuto, Y., Shirafuji, H., Yamakawa, M. and Tsuda, T. (2012). Genetic reassortment between Sathuperi and Shamonda viruses of the genus Orthobunyavirus in nature: implications for their genetic relationship to Schmallenberg virus. Archives of Virology *157*, 1611–1616.

[87] Ye, L., Shang, X., Wang, Z., Hu, F., Wang, X., Xiao, Y., Zhao, X., Liu, S., He, F., Li, F., Wang, C., Jiang, J. and Lin, J. (2015). A case of severe fever with thrombocytopenia syndrome caused by a novel bunyavirus in Zhejiang, China. International Journal of Infectious Diseases *33*, 199–201.

[88] Yi, H., Devkota, B. R., Yu, J.-s., Oh, K.-c., Kim, J. and Kim, H.-J. (2014). Effects of global warming on mosquitoes & mosquito-borne diseases and the new strategies for mosquito control. Entomological Research *44*, 215–235.

[89] Yu, L., Ye, L., Zhao, R., Liu, Y. F. and Yang, S. J. (2009). HSP70 induced by Hantavirus infection interacts with viral nucleocapsid protein and its overexpression suppresses virus infection in Vero E6 cells. American journal of translational research *1*, 367–80.

[90] Yu, X.-J., Liang, M.-F., Zhang, S.-Y., Liu, Y., Li, J.-D., Sun, Y.-L., Zhang, L., Zhang, Q.-F., Popov, V. L., Li, C., Qu, J., Li, Q., Zhang, Y.-P., Hai, R., Wu, W., Wang, Q., Zhan, F.-X., Wang, X.-J., Kan, B., Wang, S.-W., Wan, K.-L., Jing, H.-Q., Lu, J.-X., Yin, W.-W., Zhou, H., Guan, X.-H., Liu, J.-F., Bi, Z.-Q., Liu, G.-H., Ren, J., Wang, H., Zhao, Z., Song, J.-D., He, J.-R., Wan, T., Zhang, J.-S., Fu, X.-P., Sun, L.-N., Dong, X.-P., Feng, Z.-J., Yang, W.-Z., Hong, T., Zhang, Y., Walker, D. H., Wang, Y. and Li, D.-X. (2011). Fever with Thrombocytopenia Associated with a Novel Bunyavirus in China. New England Journal of Medicine *364*, 1523–1532.

Appendix

Accession	Coverage (%)	Peptides	Unique	Avg. Mass	Description
P20470	20	45	45	258668	RNA-directed RNA polymerase L OS=Bunyamwera virus OX=35304 GN=L PE=3 SV=1
A0A087WVQ6	17	26	26	192057	Clathrin heavy chain OS=Homo sapiens OX=9606 GN=CLTC PE=1 SV=1
Q00610	17	26	26	191613	Clathrin heavy chain 1 OS=Homo sapiens OX=9606 GN=CLTC PE=1 SV=5
P35580	24	52	24	228997	Myosin-10 OS=Homo sapiens OX=9606 GN=MYH10 PE=1 SV=3
P46940	13	21	19	189251	Ras GTPase-activating-like protein IQGAP1 OS=Homo sapiens OX=9606 GN=IQGAP1 PE=1 SV=1
A0A0A7KUA1	48	14	14	26664	Nucleoprotein OS=Bunyamwera virus OX=35304 PE=3 SV=1
P16495	48	14	14	26664	Nucleoprotein OS=Bunyamwera virus OX=35304 GN=N PE=1 SV=1
O00159	9	12	11	121682	Unconventional myosin-Ic OS=Homo sapiens OX=9606 GN=MYO1C PE=1 SV=4
Q01082	4	10	10	274608	Spectrin beta chain non-erythrocytic 1 OS=Homo sapiens OX=9606 GN=SPTBN1 PE=1 SV=2
A0A087WUZ3	4	10	10	274828	Spectrin beta chain OS=Homo sapiens OX=9606 GN=SPTBN1 PE=1 SV=1
Q86YZ3	5	9	9	282389	Hornerin OS=Homo sapiens OX=9606 GN=HRNR PE=1 SV=2
O75369	5	11	9	278162	Filamin-B OS=Homo sapiens OX=9606 GN=FLNB PE=1 SV=2
A0A087X0K9	7	9	9	187847	Tight junction protein ZO-1 OS=Homo sapiens OX=9606 GN=TJP1 PE=1 SV=1

Accession	Coverage (%)	Peptides	Unique	Avg. Mass	Description
G5E9E7	7	9	9	189674	Tight junction protein 1 (Zona occludens 1) isoform CRA_e OS=Homo sapiens OX=9606 GN=TJP1 PE=1 SV=1
Q07157	7	9	9	195457	Tight junction protein ZO-1 OS=Homo sapiens OX=9606 GN=TJP1 PE=1 SV=3
G3V1L9	7	9	9	197458	Tight junction protein 1 (Zona occludens 1) isoform CRA_a OS=Homo sapiens OX=9606 GN=TJP1 PE=1 SV=1
A0A087WWY3	4	8	6	245848	Filamin-A OS=Homo sapiens OX=9606 GN=FLNA PE=1 SV=1
Q60FE5	3	8	6	278224	Filamin-A OS=Homo sapiens OX=9606 GN=FLNA PE=1 SV=1
P21333	3	8	6	280737	Filamin-A OS=Homo sapiens OX=9606 GN=FLNA PE=1 SV=4
H9KV75	18	16	5	94826	Alpha-actinin-1 OS=Homo sapiens OX=9606 GN=ACTN1 PE=1 SV=1
P12814	16	16	5	103058	Alpha-actinin-1 OS=Homo sapiens OX=9606 GN=ACTN1 PE=1 SV=2
A0A087WY00	5	9	5	212200	Unconventional myosin-Va OS=Homo sapiens OX=9606 GN=MYO5A PE=1 SV=1
G3V394	5	9	5	215473	Unconventional myosin-Va OS=Homo sapiens OX=9606 GN=MYO5A PE=1 SV=1
Q9Y4I1	5	9	5	215403	Unconventional myosin-Va OS=Homo sapiens OX=9606 GN=MYO5A PE=1 SV=2
F8W6H6	5	9	5	215332	Unconventional myosin-Va OS=Homo sapiens OX=9606 GN=MYO5A PE=1 SV=2
F8WE88	5	9	5	215357	Unconventional myosin-Va OS=Homo sapiens OX=9606 GN=MYO5A PE=1 SV=2

Accession	Coverage (%)	Peptides	Unique	Avg. Mass	Description
F5H7S3	19	6	5	28525	Tropomyosin alpha-1 chain OS=Homo sapiens OX=9606 GN=TPM1 PE=1 SV=2
H7BYY1	19	6	5	28747	Tropomyosin 1 (Alpha) isoform CRA_m OS=Homo sapiens OX=9606 GN=TPM1 PE=1 SV=1
B7Z596	17	6	5	31753	Tropomyosin alpha-1 chain OS=Homo sapiens OX=9606 GN=TPM1 PE=1 SV=1
P48594	11	5	5	44854	Serpin B4 OS=Homo sapiens OX=9606 GN=SERPINB4 PE=1 SV=2
E9PDF6	4	5	5	128481	Unconventional myosin-Ib OS=Homo sapiens OX=9606 GN=MYO1B PE=1 SV=1
O43795	4	5	5	131985	Unconventional myosin-Ib OS=Homo sapiens OX=9606 GN=MYO1B PE=1 SV=3
O43707	25	25	4	104854	Alpha-actinin-4 OS=Homo sapiens OX=9606 GN=ACTN4 PE=1 SV=2
P06748	8	4	4	32575	Nucleophosmin OS=Homo sapiens OX=9606 GN=NPM1 PE=1 SV=2
Q9NZT1	32	4	4	15893	Calmodulin-like protein 5 OS=Homo sapiens OX=9606 GN=CALML5 PE=1 SV=2
P31944	14	4	4	27680	Caspase-14 OS=Homo sapiens OX=9606 GN=CASP14 PE=1 SV=2
Q13835	6	4	4	82861	Plakophilin-1 OS=Homo sapiens OX=9606 GN=PKP1 PE=1 SV=2
Q5D862	3	4	4	248072	Filaggrin-2 OS=Homo sapiens OX=9606 GN=FLG2 PE=1 SV=1
Q08554	5	4	4	99987	Desmocollin-1 OS=Homo sapiens OX=9606 GN=DSC1 PE=1 SV=2
A0A0A0MRM8	3	4	4	145015	Unconventional myosin-VI OS=Homo sapiens OX=9606 GN=MYO6 PE=1 SV=1

Accession	Coverage (%)	Peptides	Unique	Avg. Mass	Description
A0A0A0MS51	4	4	4	82526	Gelsolin OS=Homo sapiens OX=9606 GN=GSN PE=1 SV=1
A0A0A0MT01	4	4	4	84745	Gelsolin OS=Homo sapiens OX=9606 GN=GSN PE=1 SV=1
P06396	4	4	4	85697	Gelsolin OS=Homo sapiens OX=9606 GN=GSN PE=1 SV=1
Q12965	3	3	3	127062	Unconventional myosin-Ie OS=Homo sapiens OX=9606 GN=MYO1E PE=1 SV=2
A0A0D9SF54	1	3	3	282835	Spectrin alpha chain non-erythrocytic 1 OS=Homo sapiens OX=9606 GN=SPTAN1 PE=1 SV=1
Q13813	1	3	3	284538	Spectrin alpha chain non-erythrocytic 1 OS=Homo sapiens OX=9606 GN=SPTAN1 PE=1 SV=3
A0A0D9SGF6	1	3	3	287604	Spectrin alpha chain non-erythrocytic 1 OS=Homo sapiens OX=9606 GN=SPTAN1 PE=1 SV=1
P12273	18	3	3	16572	Prolactin-inducible protein OS=Homo sapiens OX=9606 GN=PIP PE=1 SV=1
Q5T750	8	3	3	26238	Skin-specific protein 32 OS=Homo sapiens OX=9606 GN=XP32 PE=1 SV=1
P31947	12	3	2	27774	14-3-3 protein sigma OS=Homo sapiens OX=9606 GN=SFN PE=1 SV=1
P11021	4	3	2	72333	Endoplasmic reticulum chaperone BiP OS=Homo sapiens OX=9606 GN=HSPA5 PE=1 SV=2
Q6WCQ1	2	2	2	116533	Myosin phosphatase Rho-interacting protein OS=Homo sapiens OX=9606 GN=MPRIP PE=1 SV=3
J3KSW8	2	2	2	95929	Myosin phosphatase Rho-interacting protein (Fragment) OS=Homo sapiens OX=9606 GN=MPRIP PE=1 SV=1
E9PMP7	2	2	2	119425	LIM domain only protein 7 (Fragment) OS=Homo sapiens OX=9606 GN=LMO7 PE=1 SV=8

Accession	Coverage (%)	Peptides	Unique	Avg. Mass	Description
H0Y424	2	2	2	121445	LIM domain only protein 7 (Fragment) OS=Homo sapiens OX=9606 GN=LMO7 PE=1 SV=8
E9PMS6	1	2	2	145423	LIM domain only protein 7 OS=Homo sapiens OX=9606 GN=LMO7 PE=1 SV=1
A0A0A0MTE2	1	2	2	158202	LIM domain only protein 7 OS=Homo sapiens OX=9606 GN=LMO7 PE=1 SV=1
E9PMT2	1	2	2	160022	LIM domain only protein 7 OS=Homo sapiens OX=9606 GN=LMO7 PE=1 SV=1
F8WD26	1	2	2	186177	LIM domain only protein 7 OS=Homo sapiens OX=9606 GN=LMO7 PE=1 SV=2
J3KP06	1	2	2	190677	LIM domain only protein 7 OS=Homo sapiens OX=9606 GN=LMO7 PE=1 SV=2
Q8WWI1	1	2	2	192694	LIM domain only protein 7 OS=Homo sapiens OX=9606 GN=LMO7 PE=1 SV=3
Q13620	2	2	2	103982	Cullin-4B OS=Homo sapiens OX=9606 GN=CUL4B PE=1 SV=4
Q7Z406	8	23	1	227868	Myosin-14 OS=Homo sapiens OX=9606 GN=MYH14 PE=1 SV=2
Q9ULV0	2	5	1	213671	Unconventional myosin-Vb OS=Homo sapiens OX=9606 GN=MYO5B PE=1 SV=3
P11142	7	4	1	70898	Heat shock cognate 71 kDa protein OS=Homo sapiens OX=9606 GN=HSPA8 PE=1 SV=1
E9PKE3	7	4	1	68806	Heat shock cognate 71 kDa protein OS=Homo sapiens OX=9606 GN=HSPA8 PE=1 SV=1

Accession	Coverage (%)	Peptides	Unique	Avg. Mass	Description
P17066	5	3	1	71028	Heat shock 70 kDa protein 6 OS=Homo sapiens OX=9606 GN=HSPA6 PE=1 SV=2
P48741	9	3	1	40244	Putative heat shock 70 kDa protein 7 OS=Homo sapiens OX=9606 GN=HSPA7 PE=5 SV=2
H0YMW4	18	3	1	16177	Annexin (Fragment) OS=Homo sapiens OX=9606 GN=ANXA2 PE=1 SV=1
P32119	9	2	1	21892	Peroxiredoxin-2 OS=Homo sapiens OX=9606 GN=PRDX2 PE=1 SV=5
E5RGE1	43	2	1	5763	14-3-3 protein zeta/delta (Fragment) OS=Homo sapiens OX=9606 GN=YWHAZ PE=1 SV=8
E5RIR4	29	2	1	8434	14-3-3 protein zeta/delta (Fragment) OS=Homo sapiens OX=9606 GN=YWHAZ PE=1 SV=1
E9PD24	24	2	1	10612	14-3-3 protein zeta/delta (Fragment) OS=Homo sapiens OX=9606 GN=YWHAZ PE=1 SV=1
E7EVZ2	22	2	1	11270	14-3-3 protein zeta/delta (Fragment) OS=Homo sapiens OX=9606 GN=YWHAZ PE=1 SV=1
E7ESK7	16	2	1	15697	14-3-3 protein zeta/delta (Fragment) OS=Homo sapiens OX=9606 GN=YWHAZ PE=1 SV=1
P63104	9	2	1	27745	14-3-3 protein zeta/delta OS=Homo sapiens OX=9606 GN=YWHAZ PE=1 SV=1
E7EX29	9	2	1	28037	14-3-3 protein zeta/delta (Fragment) OS=Homo sapiens OX=9606 GN=YWHAZ PE=1 SV=1
A0A1B0GVI3	24	2	1	10030	Keratin type I cytoskeletal 10 (Fragment) OS=Homo sapiens OX=9606 GN=KRT10 PE=1 SV=1
Q6UWP8	3	1	1	60541	Suprabasin OS=Homo sapiens OX=9606 GN=SBSN PE=1 SV=2

Accession	Coverage (%)	Peptides	Unique	Avg. Mass	Description
P25311	3	1	1	34259	Zinc-alpha-2-glycoprotein OS=Homo sapiens OX=9606 GN=AZGP1 PE=1 SV=2
P23246	2	1	1	76150	Splicing factor proline- and glutamine-rich OS=Homo sapiens OX=9606 GN=SFPQ PE=1 SV=2
Q92804	2	1	1	61830	TATA-binding protein-associated factor 2N OS=Homo sapiens OX=9606 GN=TAF15 PE=1 SV=1
A0A075B7D9	3	1	1	48840	TATA-binding protein-associated factor 2N OS=Homo sapiens OX=9606 GN=TAF15 PE=1 SV=1
P35637	3	1	1	53426	RNA-binding protein FUS OS=Homo sapiens OX=9606 GN=FUS PE=1 SV=1
H3BPE7	3	1	1	53497	RNA-binding protein FUS OS=Homo sapiens OX=9606 GN=FUS PE=1 SV=1
P00338	3	1	1	36689	L-lactate dehydrogenase A chain OS=Homo sapiens OX=9606 GN=LDHA PE=1 SV=2
P52272	1	1	1	77516	Heterogeneous nuclear ribonucleoprotein M OS=Homo sapiens OX=9606 GN=HNRNPM PE=1 SV=3
P22735	2	1	1	89787	Protein-glutamine gamma-glutamyltransferase K OS=Homo sapiens OX=9606 GN=TGM1 PE=1 SV=4
P10599	9	1	1	11737	Thioredoxin OS=Homo sapiens OX=9606 GN=TXN PE=1 SV=3
Q14574	1	1	1	99969	Desmocollin-3 OS=Homo sapiens OX=9606 GN=DSC3 PE=1 SV=3
P01861	3	1	1	35941	Immunoglobulin heavy constant gamma 4 OS=Homo sapiens OX=9606 GN=IGHG4 PE=1 SV=1
A0A286YFJ8	2	1	1	43832	Immunoglobulin heavy constant gamma 4 (Fragment) OS=Homo sapiens OX=9606 GN=IGHG4 PE=1 SV=1

Accession	Coverage (%)	Peptides	Unique	Avg. Mass	Description
P06702	11	1	1	13242	Protein S100-A9 OS=Homo sapiens OX=9606 GN=S100A9 PE=1 SV=1
P06899	6	1	1	13904	Histone H2B type 1-J OS=Homo sapiens OX=9606 GN=HIST1H2BJ PE=1 SV=3
Q99880	6	1	1	13952	Histone H2B type 1-L OS=Homo sapiens OX=9606 GN=HIST1H2BL PE=1 SV=3
O60814	6	1	1	13890	Histone H2B type 1-K OS=Homo sapiens OX=9606 GN=HIST1H2BK PE=1 SV=3
Q16778	6	1	1	13920	Histone H2B type 2-E OS=Homo sapiens OX=9606 GN=HIST2H2BE PE=1 SV=3
Q99879	6	1	1	13989	Histone H2B type 1-M OS=Homo sapiens OX=9606 GN=HIST1H2BM PE=1 SV=3
P58876	6	1	1	13936	Histone H2B type 1-D OS=Homo sapiens OX=9606 GN=HIST1H2BD PE=1 SV=2
Q93079	6	1	1	13892	Histone H2B type 1-H OS=Homo sapiens OX=9606 GN=HIST1H2BH PE=1 SV=3
P23527	6	1	1	13906	Histone H2B type 1-O OS=Homo sapiens OX=9606 GN=HIST1H2BO PE=1 SV=3
P33778	6	1	1	13950	Histone H2B type 1-B OS=Homo sapiens OX=9606 GN=HIST1H2BB PE=1 SV=2
Q5QNW6	6	1	1	13920	Histone H2B type 2-F OS=Homo sapiens OX=9606 GN=HIST2H2BF PE=1 SV=3
Q99877	6	1	1	13922	Histone H2B type 1-N OS=Homo sapiens OX=9606 GN=HIST1H2BN PE=1 SV=3
P57053	6	1	1	13944	Histone H2B type F-S OS=Homo sapiens OX=9606 GN=H2BFS PE=1 SV=2
P62807	6	1	1	13906	Histone H2B type 1-C/E/F/G/I OS=Homo sapiens OX=9606 GN=HIST1H2BC PE=1 SV=4
U3KQK0	4	1	1	18804	Histone H2B OS=Homo sapiens OX=9606 GN=HIST1H2BN PE=1 SV=1
Q15828	7	1	1	16511	Cystatin-M OS=Homo sapiens OX=9606 GN=CST6 PE=1 SV=1

Accession	Coverage (%)	Peptides	Unique	Avg. Mass	Description
P05090	6	1	1	21276	Apolipoprotein D OS=Homo sapiens OX=9606 GN=APOD PE=1 SV=1
C9JF17	5	1	1	24158	Apolipoprotein D (Fragment) OS=Homo sapiens OX=9606 GN=APOD PE=1 SV=1
Q16643	3	1	1	71429	Drebrin OS=Homo sapiens OX=9606 GN=DBN1 PE=1 SV=4
D6R9Q9	5	1	1	41448	Drebrin OS=Homo sapiens OX=9606 GN=DBN1 PE=1 SV=1
K7ERX7	8	1	1	21590	ATP synthase subunit alpha mitochondrial (Fragment) OS=Homo sapiens OX=9606 GN=ATP5F1A PE=1 SV=1
Q9H2K2	1	1	1	126918	Tankyrase-2 OS=Homo sapiens OX=9606 GN=TNKS2 PE=1 SV=1
D6RD46	1	1	1	109935	LIM and calponin homology domains-containing protein 1 OS=Homo sapiens OX=9606 GN=LIMCH1 PE=1 SV=1
Q9UPQ0	1	1	1	121867	LIM and calponin homology domains-containing protein 1 OS=Homo sapiens OX=9606 GN=LIMCH1 PE=1 SV=4
O14974	1	1	1	115281	Protein phosphatase 1 regulatory subunit 12A OS=Homo sapiens OX=9606 GN=PPP1R12A PE=1 SV=1
H0YIS3	4	1	1	27032	Protein phosphatase 1 regulatory subunit 12A (Fragment) OS=Homo sapiens OX=9606 GN=PPP1R12A PE=1 SV=1
H3BTJ2	8	1	1	18477	Pyruvate kinase PKM (Fragment) OS=Homo sapiens OX=9606 GN=PKM PE=1 SV=1
H3BQ34	5	1	1	30720	Pyruvate kinase OS=Homo sapiens OX=9606 GN=PKM PE=1 SV=1
B4DNK4	3	1	1	49898	Pyruvate kinase OS=Homo sapiens OX=9606 GN=PKM PE=1 SV=1
H3BTN5	3	1	1	53045	Pyruvate kinase (Fragment) OS=Homo sapiens OX=9606 GN=PKM PE=1 SV=1

Accession	Coverage (%)	Peptides	Unique	Avg. Mass	Description
P14618	2	1	1	57937	Pyruvate kinase PKM OS=Homo sapiens OX=9606 GN=PKM PE=1 SV=4
H3BU13	16	1	1	8951	Pyruvate kinase PKM (Fragment) OS=Homo sapiens OX=9606 GN=PKM PE=1 SV=1
H3BT25	9	1	1	16427	Pyruvate kinase PKM (Fragment) OS=Homo sapiens OX=9606 GN=PKM PE=1 SV=1
H3BUW1	8	1	1	17820	Pyruvate kinase PKM (Fragment) OS=Homo sapiens OX=9606 GN=PKM PE=1 SV=1
A0A1B0GTW1	1	1	1	140727	Tight junction protein ZO-2 OS=Homo sapiens OX=9606 GN=TJP2 PE=1 SV=1
A0A2R8YDH4	1	1	1	147881	Tight junction protein ZO-2 OS=Homo sapiens OX=9606 GN=TJP2 PE=3 SV=1
Q9UDY2	1	1	1	133958	Tight junction protein ZO-2 OS=Homo sapiens OX=9606 GN=TJP2 PE=1 SV=2
A0A0G2JS82	1	1	1	101659	AP-2 complex subunit alpha-2 (Fragment) OS=Homo sapiens OX=9606 GN=AP2A2 PE=1 SV=1
O94973	1	1	1	103960	AP-2 complex subunit alpha-2 OS=Homo sapiens OX=9606 GN=AP2A2 PE=1 SV=2
O95782	1	1	1	107546	AP-2 complex subunit alpha-1 OS=Homo sapiens OX=9606 GN=AP2A1 PE=1 SV=3
A0A0G2JQM1	1	1	1	70827	AP-2 complex subunit alpha-2 (Fragment) OS=Homo sapiens OX=9606 GN=AP2A2 PE=1 SV=1
M9MMK7	1	1	1	50892	Dynein heavy chain 14 axonemal OS=Homo sapiens OX=9606 GN=DNAH14 PE=1 SV=1
Q0VDD8	0	1	1	399896	Dynein heavy chain 14 axonemal OS=Homo sapiens OX=9606 GN=DNAH14 PE=2 SV=3

Accession	Coverage (%)	Peptides	Unique	Avg. Mass	Description
C9J8U1	1	1	1	88182	Cytospin-A (Fragment) OS=Homo sapiens OX=9606 GN=SPECC1L PE=4 SV=8
Q8WVV4	2	1	1	68065	Protein POF1B OS=Homo sapiens OX=9606 GN=POF1B PE=1 SV=3
Q13045	1	1	1	144751	Protein flightless-1 homolog OS=Homo sapiens OX=9606 GN=FLII PE=1 SV=2
Q15149	0	1	1	531796	Plectin OS=Homo sapiens OX=9606 GN=PLEC PE=1 SV=3
O60218	3	1	1	36020	Aldo-keto reductase family 1 member B10 OS=Homo sapiens OX=9606 GN=AKR1B10 PE=1 SV=2
A0A087WVQ9	2	1	1	47883	Elongation factor 1-alpha 1 OS=Homo sapiens OX=9606 GN=EEF1A1 PE=1 SV=1
P68104	2	1	1	50141	Elongation factor 1-alpha 1 OS=Homo sapiens OX=9606 GN=EEF1A1 PE=1 SV=1
Q5VTE0	2	1	1	50185	Putative elongation factor 1-alpha-like 3 OS=Homo sapiens OX=9606 GN=EEF1A1P5 PE=5 SV=1
Q05639	2	1	1	50470	Elongation factor 1-alpha 2 OS=Homo sapiens OX=9606 GN=EEF1A2 PE=1 SV=1
A0A2U3TZH3	2	1	1	54341	Elongation factor 1-alpha 2 OS=Homo sapiens OX=9606 GN=EEF1A2 PE=4 SV=1
K7EKN2	3	1	1	22514	Beta-enolase (Fragment) OS=Homo sapiens OX=9606 GN=ENO3 PE=1 SV=1
A0A2R8Y6G6	1	1	1	47327	Alpha-enolase OS=Homo sapiens OX=9606 GN=ENO1 PE=1 SV=1
A4D1T9	3	1	1	26445	Probable inactive serine protease 37 OS=Homo sapiens OX=9606 GN=PRSS37 PE=1 SV=1

Accession	Coverage (%)	Peptides	Unique	Avg. Mass	Description
Q9NZI8	2	1	1	63481	Insulin-like growth factor 2 mRNA-binding protein 1 OS=Homo sapiens OX=9606 GN=IGF2BP1 PE=1 SV=2
Q8IVT2	1	1	1	75357	Mitotic interactor and substrate of PLK1 OS=Homo sapiens OX=9606 GN=MISP PE=1 SV=1
tr—F5H2D0	1	1	1	76614	Complement C1r subcomponent OS=Homo sapiens OX=9606 GN=C1R PE=1 SV=3
P00736	1	1	1	80119	Complement C1r subcomponent OS=Homo sapiens OX=9606 GN=C1R PE=1 SV=2
B4DPQ0	1	1	1	81890	cDNA FLJ54471 highly similar to Complement C1r subcomponent (EC 3.4.21.41) OS=Homo sapiens OX=9606 GN=C1R PE=1 SV=1
A0A096LNW4	2	1	1	55232	PRAME family member 9/15 OS=Homo sapiens OX=9606 GN=PRAMEF9 PE=4 SV=1
S4R3H4	0	1	1	145442	Apoptotic chromatin condensation inducer in the nucleus OS=Homo sapiens OX=9606 GN=ACIN1 PE=1 SV=1
E7EQT4	0	1	1	147362	Apoptotic chromatin condensation inducer in the nucleus OS=Homo sapiens OX=9606 GN=ACIN1 PE=1 SV=2
Q9UKV3	0	1	1	151861	Apoptotic chromatin condensation inducer in the nucleus OS=Homo sapiens OX=9606 GN=ACIN1 PE=1 SV=2
A0A087X223	1	1	1	61245	Sterile alpha motif domain-containing protein 11 OS=Homo sapiens OX=9606 GN=SAMD11 PE=1 SV=1
Q96PE2	0	1	1	221671	Rho guanine nucleotide exchange factor 17 OS=Homo sapiens OX=9606 GN=ARHGEF17 PE=1 SV=1
P55060	1	1	1	110417	Exportin-2 OS=Homo sapiens OX=9606 GN=CSE1L PE=1 SV=3

Accession	Coverage (%)	Peptides	Unique	Avg. Mass	Description
E5RIF2	0	1	1	145614	Brefeldin A-inhibited guanine nucleotide-exchange protein 1 (Fragment) OS=Homo sapiens OX=9606 GN=ARFGEF1 PE=1 SV=2
Q9Y6D6	0	1	1	208766	Brefeldin A-inhibited guanine nucleotide-exchange protein 1 OS=Homo sapiens OX=9606 GN=ARFGEF1 PE=1 SV=2
Q9Y6D5	0	1	1	202037	Brefeldin A-inhibited guanine nucleotide-exchange protein 2 OS=Homo sapiens OX=9606 GN=ARFGEF2 PE=1 SV=3
P0C869	1	1	1	87978	Cytosolic phospholipase A2 beta OS=Homo sapiens OX=9606 GN=PLA2G4B PE=1 SV=2
Q6EMB2	0	1	1	143577	Tubulin polyglutamylase TTLL5 OS=Homo sapiens OX=9606 GN=TTLL5 PE=1 SV=3
H7BY79	2	1	1	49043	Cadherin-like protein 26 (Fragment) OS=Homo sapiens OX=9606 GN=CDH26 PE=1 SV=1